Gö-VIP- 20: Francesca Odoardi & Alexander Flügel

Name der Einrichtung: Institut für Neuroimmunologie und Multiple-Sklerose-Forschung, Universitätsmedizin Göttingen

Titel der Publikation: β-synuclein reactive T cells induce autoimmune CNS grey matter degeneration.

In: Nature 2019 Feb; 566 (7745): 503-508.

Autoren: D. Lodygin*, M. Hermann*, N. Schweingruber, C. Flügel-Koch, T. Watanabe, **C. Schlosser, A. Merlini, H. Körner, H.-F. Chang, H.J. Fischer**, H.M. Reichardt, M. Zagrebelsky, B. Mollenhauer, J. Frahm, C. Stadelmann, S. Kügler, D. Fitzner, **M. Haberl, F. Odoardi*, A. Flügel*#** (2019)

*contributed equally, # correspondence

D. Lodygin, M. Hermann, N. Schweingruber, C. Schlosser, A. Merlini, H. Körner, H.-F. Chang, H.J. Fischer, H.M., M. Haberl, F. Odoardi, A. Flügel: Institute for Neuroimmunology and Multiple Sclerosis Research, University Medical Center Göttingen, Germany

C. Flügel-Koch: Institute for Anatomy II, Friedrich-Alexander-University, Erlangen, Germany

T. Watanabe, J. Frahm: Biomedizinische NMR, Max-Planck-Institut für biophysikalische Chemie, Göttingen, Germany

H.M. Reichardt. Institute for Cellular and Molecular Immunology, University Medical Center Göttingen, Germany

M. Zagrebelsky: Zoological Institute, Division of Cellular Neurobiology, TU Braunschweig, Germany

B. Mollenhauer: Paracelsus-Elena-Klinik Kassel, Germany

S. Kügler, D. Fitzner: Institute for Neurology, University Medical Center Göttingen, Germany

C. Stadelmann: Institute for Neuropathology, University Medical Center Göttingen

F. Odoardi: Center for Biostructural Imaging of Neurodegeneration, Germany

Zusammenfassung des wissenschaftlichen Inhalts

(Francesca Odoardi & Alexander Flügel)

Die Studie befasst sich mit der Frage, wie das Immunsystem die graue Substanz des Gehirns angreift. Die graue Substanz ist die zentrale Schalt- und Speicherzentrale des Gehirns. Informationen, die über Nervenfortsätze der weißen Hirnsubstanz weitergeleitet werden, werden hier verschaltet und verarbeitet. Dieses Gewebe stellt daher eine Art Achillesferse unseres Gehirns dar. Schäden in diesem Bereich können gravierende

neuropsychiatrischen Störungen zur Folge haben. Dies zeigt sich besonders deutlich bei degenerativen Krankheiten unseres Gehirns, wie der Alzheimer- oder Parkinson‘schen Erkrankung. Bei der Autoimmunerkrankung Multiplen Sklerose ging man traditionell davon aus, dass vornehmlich die weiße Hirnsubstanz vom Krankheitsprozess betroffen ist. Kürzlich stellte sich allerdings heraus, dass auch die graue Hirnsubstanz durch den Entzündungsprozess erheblich geschädigt wird. In der Tat sind Symptome einer Schädigung der grauen Substanz wie kognitive Störungen, Müdigkeit und Krampfanfälle bei Patienten mit Multipler Sklerose regelmäßig anzutreffen. Derzeit verfügbare experimentelle Modelle befallen vorwiegend die weiße Substanz des Rückenmarks. Diese Diskrepanz zwischen Tiermodell und menschlicher Erkrankung ist ein starkes Handicap für die Multiple Sklerose-Forschung, da die Entzündung und Degeneration der grauen Hirnsubstanz die treibende Kraft für die chronisch voranschreitende MS, welche die Patienten am stärksten belastet und für die es bisher keine wirksame Behandlungsmöglichkeit gibt, darstellen. Somit war ein sehr wichtiger Aspekt der Multiplen Sklerose für die experimentelle Forschung unzugänglich.

In dieser Studie wurde die überraschende Beobachtung gemacht, dass T-Zellen, die gegen das neuronale Autoantigen Beta-Synuklein gerichtet sind, in Ratten eine starke Entzündung der grauen Hirnsubstanz auslösen. Wiederholte Angriffe durch diese pathogenen T-Zellen führten zu ausgedehnten degenerativen Veränderungen der grauen Hirnsubstanz. Mit diesem neuen Modell kann daher jetzt erstmals im Detail untersucht werden, welche Mechanismen und Faktoren T-Zellen dazu befähigen, in die graue Substanz des Gehirns einzudringen und eine fortschreitende Neurodegeneration auszulösen. In der Studie wurden zudem erste Hinweise dafür gefunden, dass Beta-Synuklein-gerichtete T-Zellen auch in der Pathogenese der Multiplen Sklerose eine Rolle spielen könnten. Patienten mit chronisch-fortschreitendem Krankheitsverlauf wiesen eine signifikant erhöhte Anzahl Beta-Synuklein-reaktiver T-Zellen in ihrem Blut auf. Die Ergebnisse dieser Arbeit könnten somit nicht nur für die Grundlagenforschung von Bedeutung sein, sondern auch neue Wege für klinische Anwendungen weisen.

Weitere Informationen:
Dr. Francesca Odoardi & Prof. Dr. Alexander Flügel
Universitätsmedizin Göttingen
Institut für Neuroimmunologie und Multiple Sklerose Forschung
Anschrift: Von-Siebold-Str. 3a, 37075 Göttingen
Telefon: 0551/61158
Email: IMSF@med.uni-goettingen.de

ARTICLE

Corrected: Publisher Correction

https://doi.org/10.1038/s41586-019-0964-2

β-Synuclein-reactive T cells induce autoimmune CNS grey matter degeneration

Dmitri Lodygin[1,10], Moritz Hermann[1,10], Nils Schweingruber[1], Cassandra Flügel-Koch[2], Takashi Watanabe[3], Corinna Schlosser[1], Arianna Merlini[1], Henrike Körner[1], Hsin-Fang Chang[1], Henrike J. Fischer[1], Holger M. Reichardt[4], Marta Zagrebelsky[5], Brit Mollenhauer[6,7], Sebastian Kügler[7], Dirk Fitzner[7], Jens Frahm[3], Christine Stadelmann[8], Michael Haberl[1], Francesca Odoardi[1,9,11]* & Alexander Flügel[1,11]*

The grey matter is a central target of pathological processes in neurodegenerative disorders such as Parkinson's and Alzheimer's diseases. The grey matter is often also affected in multiple sclerosis, an autoimmune disease of the central nervous system. The mechanisms that underlie grey matter inflammation and degeneration in multiple sclerosis are not well understood. Here we show that, in Lewis rats, T cells directed against the neuronal protein β-synuclein specifically invade the grey matter and that this is accompanied by the presentation of multifaceted clinical disease. The expression pattern of β-synuclein induces the local activation of these T cells and, therefore, determined inflammatory priming of the tissue and targeted recruitment of immune cells. The resulting inflammation led to significant changes in the grey matter, which ranged from gliosis and neuronal destruction to brain atrophy. In humans, β-synuclein-specific T cells were enriched in patients with chronic-progressive multiple sclerosis. These findings reveal a previously unrecognized role of β-synuclein in provoking T-cell-mediated pathology of the central nervous system.

The complex neuronal networks of the grey matter in the central nervous system (CNS) constitute the site at which the signals for body control are received, processed and distributed. Consequently, any damage to this neuronal fulcrum has a most severe and enduring impact on the integrity and function of the CNS, as is seen in chronic neurodegeneration of the brain in disorders such as Parkinson's and Alzheimer's diseases. In multiple sclerosis (MS), an autoimmune disease of the CNS, it is not only the myelinated white matter that is affected by the autoimmune attack, as previously thought[1–3], but also the grey matter. In fact, it is the destruction of the grey matter that is primarily responsible for the brain atrophy and disease progression observed in MS[4]. An important gap in our understanding of the pathogenesis of MS results from the fact that the currently available experimental models—in particular, experimental autoimmune encephalomyelitis (EAE)—do not reproduce this critical hallmark of the human disease. The target autoantigens of classical EAE models are generally myelin proteins, such as myelin basic protein (MBP), myelin oligodendrocyte glycoprotein or proteolipid protein[5]. These proteins are predominantly expressed in CNS white matter, in which the EAE lesions are also located.

β-Synuclein-specific T cells induce grey matter disease

Here we studied T cells specific for β-synuclein, which is abundantly present within neuronal synapses[6] and has previously been proposed to be a potential CNS autoimmune target antigen[7]. T cell lines specific for β-synuclein and for MBP were established and labelled with fluorescent proteins by retroviral gene transfer ($T_{β\text{-syn}}$ and T_{MBP} cells, respectively) (Extended Data Fig. 1a–c). After intravenous transfer into healthy recipient rats, T_{MBP} cells infiltrated the white matter of the spinal cord and the brain, as expected, and evoked the typical monophasic EAE characterized by ascending paresis and weight loss[8,9]. $T_{β\text{-syn}}$ cells were also highly pathogenic. However, in notable contrast to T_{MBP} cells, the $T_{β\text{-syn}}$ cells almost exclusively invaded the grey matter, and in particular the cerebral cortex, an area that is almost devoid of T_{MBP} cells in EAE (Fig. 1a and Extended Data Fig. 1d). Clinically, the rats developed a very heterogeneous disease phenotype that included atypical signs such as paresis of individual limbs, head tilting and ataxia (Extended Data Fig. 1e, f).

Our T cell lines consist of polyclonal populations with potentially distinct T cell receptor (TCR) reactivity (Extended Data Fig. 1g). To ascertain whether β-synuclein acted as the target autoantigen for the observed grey matter disease, we generated a TCR-transgenic rat, which had an immune repertoire that mainly (over 95%) contained T cells that were reactive against β-synuclein (Fig. 1b, c and Extended Data Fig. 1h, i). T cell lines from these TCR-transgenic rats (Extended Data Fig. 1j–o) induced massive grey matter lesions similar to wild-type $T_{β\text{-syn}}$ cells, and the majority of rats (more than 80%) displayed an atypical disease characterized by paroxysmal bouts of monotonous scratching movements, jerks, pareses and ataxic and/or rotational movements (Fig. 1d, Extended Data Fig. 1p and Supplementary Video 1).

Migratory paths and cues of $T_{β\text{-syn}}$ cells

Disease signs induced by $T_{β\text{-syn}}$ cells started, similarly to EAE induced by T_{MBP} cells, after a preclinical phase of two to three days after T cell transfer (Extended Data Fig. 1q). During this prodromal phase, $T_{β\text{-syn}}$ cells—as do T_{MBP} cells[8,10]—travelled along a defined route through the lung, mediastinal lymph nodes, spleen and blood before they arrived at the CNS. On their way, the $T_{β\text{-syn}}$ cells assumed a migratory mode; that is, they showed downregulation of activation markers and concurrent upregulation of chemokine receptors and adhesion molecules that are required for crossing the blood–brain barrier (BBB)[10] (Extended

[1]Institute for Neuroimmunology and Multiple Sclerosis Research, University Medical Center Göttingen, Göttingen, Germany. [2]Institute of Functional and Clinical Anatomy, Friedrich-Alexander-University Erlangen-Nürnberg, Erlangen, Germany. [3]Biomedizinische NMR, Max-Planck-Institut für biophysikalische Chemie, Göttingen, Germany. [4]Institute for Cellular and Molecular Immunology, University Medical Center Göttingen, Göttingen, Germany. [5]Zoological Institute, Division of Cellular Neurobiology, Technical University Braunschweig, Braunschweig, Germany. [6]Paracelsus-Elena-Klinik Kassel, Kassel, Germany. [7]Institute for Neurology, University Medical Center Göttingen, Göttingen, Germany. [8]Institute for Neuropathology, University Medical Center Göttingen, Göttingen, Germany. [9]Center for Biostructural Imaging of Neurodegeneration, Göttingen, Germany. [10]These authors contributed equally: Dmitri Lodygin, Moritz Hermann. [11]These authors jointly supervised this work: Francesca Odoardi, Alexander Flügel. *e-mail: odoardi@med.uni-goettingen.de; fluegel@med.uni-goettingen.de

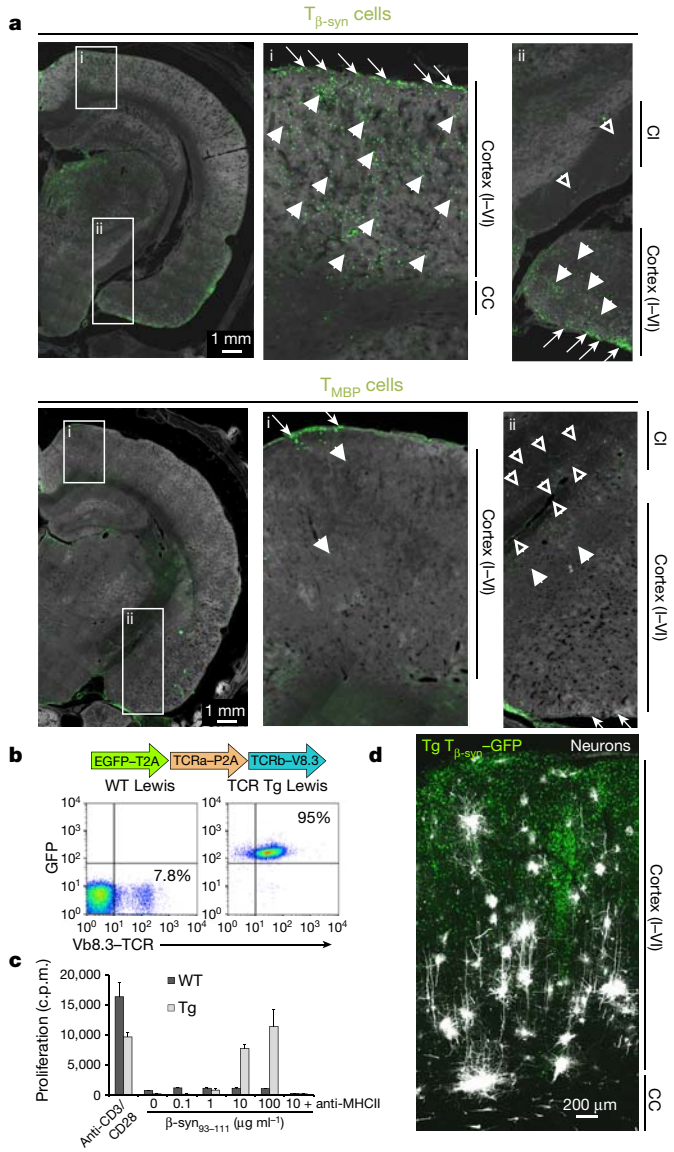

Fig. 1 | T cells specific for β-synuclein induce a CNS grey matter disease. a, Brain infiltration patterns of $T_{β\text{-}syn\text{–}GFP}$ cells (top) or $T_{MBP\text{–}GFP}$ cells (bottom). Fluorescence images of coronal brain sections at the peak of T cell invasion. Arrows, closed arrowheads and open arrowheads point to T cells (green) that accumulate in the meninges, grey matter and white matter, respectively. CC, corpus callosum; CI, capsula interna. **b**, TCR transgene construct (top) and the abundance of Vβ8.3 chain and GFP expression (bottom) in TCR transgenic compared to wild-type lymph node T cells. **c**, Proliferative response of lymph node cells of wild-type (WT) and transgenic (Tg) rats to $β\text{-synuclein}_{93–111}$.Thymidine incorporation. c.p.m., counts per min. Data are mean + s.d. Treatments with anti-CD3/CD28 and anti-MHC class II (MHCII) monoclonal antibodies were used for unspecific stimulation and to block antigen presentation, respectively. **d**, Cortical brain lesions induced by transfer of transgenic $T_{β\text{-}syn}$ cells (green). Representative confocal image of a coronal brain slice with DiI-labelled neurons (white).

Data Fig. 2a, b). Intravital two-photon laser-scanning microscopy recordings revealed that the $T_{β\text{-}syn}$ cells accumulated at the leptomeninges before disease onset (Fig. 2a and Extended Data Fig. 2a). At the same time as the start of clinical signs, $T_{β\text{-}syn}$ cells invaded deep into the adjacent cortical grey matter (Fig. 1d, Extended Data Fig. 1p and Supplementary Video 2). The peak of $T_{β\text{-}syn}$ cell infiltration was reached shortly after the manifestation of clinical signs. Thereafter, $T_{β\text{-}syn}$ cell numbers rapidly declined (Extended Data Fig. 2a). T_{MBP} cells also used the CNS-encasing leptomeninges as the point of entry; however, they were substantially confined to the spinal cord (Fig. 2a, Extended Data Fig. 2a and Supplementary Video 2).

The intravascular motility pattern did not explain the different migratory targets of $T_{β\text{-}syn}$ and T_{MBP} cells: both types of T cells rolled along or interacted more tightly with the vascular walls of brain and spinal cord vessels—that is, after fixed adherence, the cells crawled with comparable velocity along the endothelium[11] (Extended Data Fig. 2c, d and Supplementary Video 3). Even CNS-ignorant ovalbumin-specific T cells (T_{OVA} cells) had similar intravascular locomotion behaviour (Supplementary Video 4).

Previous reports have suggested that different cytokine and integrin profiles could direct T cells into different CNS regions. T helper 17 (T_H17) cells invaded the brain using LFA-1, whereas T_H1 cells entered the spinal cord through VLA-4 integrin[12–15]. Transcriptome analyses revealed that $T_{β\text{-}syn}$ and T_{MBP} cells had almost identical expression patterns of master transcription factors, cytokines, cytokine and chemokine receptors, and adhesion molecules (Fig. 2b and Extended Data Fig. 2e). The cells expressed IFNγ and IL-17 (Extended Data Fig. 1o), LFA-1 and VLA-4, and CCR6 and CXCR3, indicating a mixed T_H1/T_H17 cell type. Their chemotactic responsiveness was almost identical (Extended Data Fig. 2f). As in T_{MBP} cells[11], VLA-4 but not LFA-1 was crucial for $T_{β\text{-}syn}$ cell invasion of the CNS. VLA-4 monoclonal antibodies almost completely abolished $T_{β\text{-}syn}$ cell rolling and crawling along brain vessels, as well as subsequent grey matter invasion and disease progression (Fig. 2c, Extended Data Fig. 2g–m and Supplementary Video 5). Interference with IFNγ and, to a lesser extent, IL-17 signalling reduced the entry of $T_{β\text{-}syn}$ cells into CNS tissue and ameliorated the disease (Fig. 2c and Extended Data Fig. 2n, o).

T cell activation drives grey matter inflammation

Because the differences in the migratory properties or adhesion molecule and cytokine profiles of the T cells could not explain the preferential targeting of the grey or white matter, we next investigated whether the distribution of CNS antigens regulates invasion. Whereas MBP is predominantly expressed within highly myelinated white matter, β-synuclein is mainly expressed in grey matter with its high density of neuronal processes and synapses[16]. $T_{β\text{-}syn}$ cells accumulated mainly in areas of high β-synuclein expression (Extended Data Fig. 3a–c). Thus, antigen expression could lead to preferential T cell activation within distinct brain regions. Indeed, $T_{β\text{-}syn}$ cells isolated from the leptomeninges and, in particular, from the brain parenchyma displayed an activatory gene profile. Vice versa, T_{MBP} cells were activated mainly within the spinal cord white matter and significantly less so within the grey matter (Extended Data Fig. 4a–g). Using nuclear translocation of the fluorescently labelled nuclear factor of activated T cells (NFAT) as an activation-dependent biosensor[17,18], we could confirm $T_{β\text{-}syn}$ cell activation within the meninges and deep within the grey matter (Fig. 3a, b, Extended Data Fig. 4h–k and Supplementary Video 6).

The dominant pattern of activation of $T_{β\text{-}syn}$ cells within the grey matter indicates that β-synuclein is preferentially presented in grey matter tissue. In fact, grey-matter-derived microglia induced a stronger activation response in $T_{β\text{-}syn}$ cells than did microglia from whole-brain tissue, the latter of which also contained microglial cells from the white matter of the brain. In the presence of the appropriate neuronal or myelin antigen, microglia from the grey matter or whole-brain tissue equally stimulated both $T_{β\text{-}syn}$ and T_{MBP} cells. As expected, T_{OVA} cells were not activated by the CNS antigen-presenting cells (APCs). Blockade of the interaction between TCRs and MHC class II by monoclonal antibodies prevented the activation of $T_{β\text{-}syn}$ cells (Fig. 3c and Extended Data Fig. 5a).

The relevance of in situ activation of $T_{β\text{-}syn}$ cells was supported by the following findings. Intrathecal application of anti-MHC class II monoclonal antibodies decreased $T_{β\text{-}syn}$ cell activation in the CNS, $T_{β\text{-}syn}$ cell recruitment and clinical disease (Fig. 3d and Extended Data Fig. 5b–d). Interference with the $T_{β\text{-}syn}$ cell-signalling cascade through treatment with FK506, which prevents nuclear NFAT translocation, resulted in very similar effects (Fig. 3d and Extended Data Fig. 5e–g). By contrast, promotion of T cell activation had the opposite effect. Even

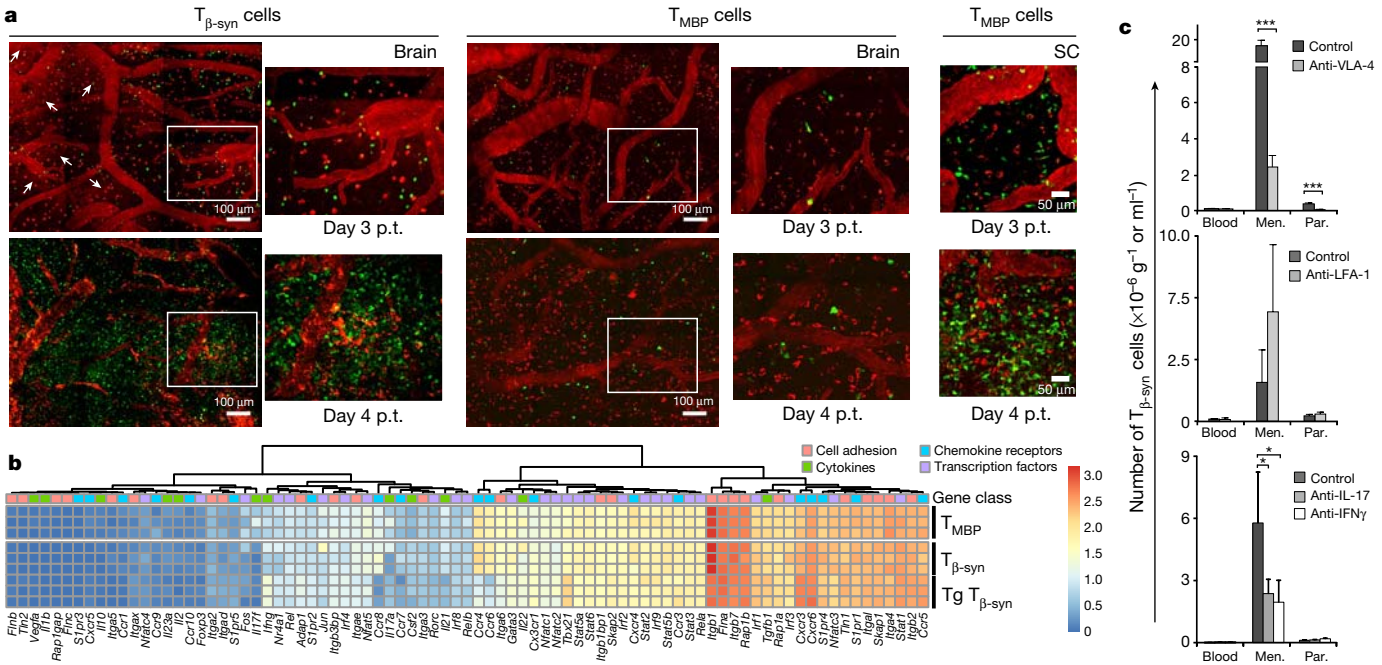

Fig. 2 | Trafficking properties and expression profiles of $T_{β\text{-syn}}$ and T_{MBP} cells. a, Leptomeninges represent entry points for $T_{β\text{-syn}}$ and T_{MBP} cells into the CNS tissues. Left and middle, $T_{β\text{-syn}}$ but not T_{MBP} cells accumulate in the leptomeninges of the brain before invading the adjacent cortical grey matter. Right, T_{MBP} cells use leptomeninges of the spinal cord (SC) to invade the white matter parenchyma. Representative two-photon laser-scanning microscopy recordings at the onset (day 3 post transfer (p.t.)) and peak (day 4 p.t.) of T cell infiltration. Green, antigen-specific T cells; red, blood vessels and meningeal macrophages. Arrows indicate areas of dye leakage. **b**, Transcriptional profiles of $T_{β\text{-syn}}$ and T_{MBP} cells from blood 3 days p.t. Heat map shows hierarchically clustered expression values (log_{10}-transformed RPKM (reads per kilobase per million mapped reads) of genes related to cell migration. Each line represents a biological replicate with $n = 3$–5 rats. **c**, Effects of blocking integrins and cytokines on entry of $T_{β\text{-syn}}$ cells into the brain. Flow cytometry analysis of the absolute number of $T_{β\text{-syn}}$ cells in blood, brain meninges (Men.) or parenchyma (Par.) at the onset of invasion in rats treated with anti-VLA-4, anti-LFA-1 or isotype-control monoclonal antibodies. Data are mean mean + s.e.m., $n = 9$ rats per group from 3 experiments. For anti-IL-17A and anti-IFNγ monoclonal antibody and PBS (control) treatment, analysis was performed at the peak of T cell infiltration. Data are mean + s.e.m., $n = 6$ rats per group from 2 experiments. Unpaired two-tailed *t*-test. $^*P < 0.05$, $^{***}P < 0.001$.

brain antigen-irrelevant T cells could be guided into the brain tissue. To achieve this, we used T_{OVA} cells, which carried a chimeric antigen receptor (Extended Data Fig. 6a, b), that were stimulated by local application of CAR crosslinking monoclonal antibodies—thus avoiding the need for the local antigen presentation machinery. Involving CNS APCs in the T cell activation process by local ovalbumin application uniformly triggered increased invasion of T_{OVA} cells (Extended Data Fig. 6c). Furthermore, local application of MBP redirected white matter-affine T_{MBP} cells into the brain cortex (Extended Data Fig. 6d). Additionally, invasion of $T_{β\text{-syn}}$ cells could be enhanced by increasing the availability of the autoantigen by neuronal overexpression of β-synuclein using viral gene transfer (Extended Data Fig. 6e–g).

The activation of $T_{β\text{-syn}}$ cells triggered an inflammatory reaction of endothelial cells and the grey matter parenchyma with significant upregulation of adhesion molecules and chemokines (Fig. 4a, b). As a consequence, strong recruitment of host T cells and myeloid cells was observed (Extended Data Fig. 7a). The correlations between effector T cell activation, local tissue response and subsequent cell recruitment also became evident in studies in which $T_{β\text{-syn}}$ and T_{OVA} cells were transferred together. When transferred alone, very few T_{OVA} cells entered the leptomeninges. After transfer with $T_{β\text{-syn}}$ cells, however, numerous T_{OVA} cells were recruited to the cortical leptomeninges and parenchyma. Their location, migratory properties and kinetics in the grey matter resembled those of $T_{β\text{-syn}}$ cells, although their activation state remained low (Extended Data Fig. 7b–d and Supplementary Video 7). Interfering with $T_{β\text{-syn}}$ cell activation efficiently reduced tissue inflammation and T_{OVA} cell recruitment (Extended Data Figs. 5d, 7e, f).

$T_{β\text{-syn}}$ cells induce permanent neurodegeneration

We next analysed the consequences of $T_{β\text{-syn}}$-cell-driven autoimmune attacks for the grey matter, which in its healthy state is almost devoid of any peripheral immune cells. Gadolinium (Gd)-enhanced magnetic resonance imaging (MRI) revealed marked signal increases in the meninges and within the cortex during disease onset, which indicates a substantial leakiness of the BBB. Intravital two-photon laser-scanning microscopy analyses after MRI confirmed these findings. Furthermore, subsequent histological analysis revealed a strong inflammatory response in the regions with Gd leakage (Fig. 5a, Extended Data Fig. 8a–d and Supplementary Video 8).

$T_{β\text{-syn}}$ cells within the grey matter crawled at high speed (around 10 µm min^{-1}) through the dense parenchyma (Extended Data Fig. 8e–h and Supplementary Video 2) and were regularly found to be in close association with neuronal structures. Some cells were even located within neurons (emperipolesis), which suggests neuronal damage[19,20] (Fig. 5b, c and Supplementary Video 9). In fact, in addition to significant glial activation—upregulation of IBA1 associated with significant morphological changes in microglia—we found signs of neuronal damage, such as a significant reduction in synaptic spines and the emergence of apoptotic neurons (Fig. 5c and Extended Data Fig. 8i–m). Most of the inflammatory changes disappeared after recovery from the acute autoimmune attack (Fig. 5a and Extended Data Fig. 8l, m).

Patients with MS generally develop multiple disease bouts with clinical remissions between relapses. This could faithfully be reproduced in our rat model by performing consecutive transfers of effector T cells in the TCR-transgenic hosts (Extended Data Fig. 9a–d). Morphological analyses three weeks after the peak from a fourth $T_{β\text{-syn}}$-cell-induced disease bout showed that—similarly to the recovery state after an acute lesion—the strong inflammation of the grey matter had almost completely vanished. Only single groups of T cells remained around vessels or within the leptomeninges and the adjacent parenchyma (Extended Data Fig. 9e). However, in contrast to the recovery state after a single inflammatory bout, we found significant persisting gliosis

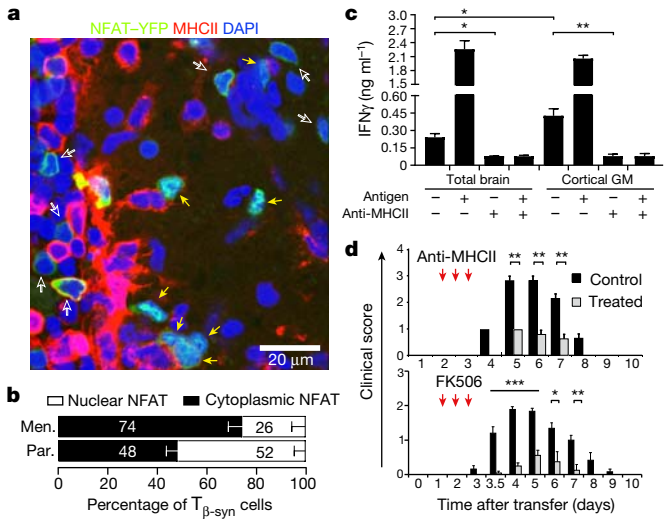

Fig. 3 | Local activation of $T_{β\text{-syn}}$ cells triggers their invasion into the CNS grey matter. a, Nuclear translocation of NFAT in $T_{β\text{-syn–NFAT–YFP}}$ cells in situ. Representative confocal image showing T cells within the cortical parenchyma in contact with MHC class II^+ cells. Filled and open arrows, $T_{β\text{-syn}}$ cells with nuclear (that is, activated) and cytosolic (that is, not activated) NFAT, respectively. **b**, Quantification of activated T cells in the meningeal and cortical grey matter. Data are mean ± s.d. of a total 4,400 cells from 2 different experiments. **c**, Grey-matter-derived microglia function as APCs for $T_{β\text{-syn}}$ cells. IFNγ production by $T_{β\text{-syn}}$ cells stimulated by microglia from total brain or cortical grey matter with or without the presence of cognate antigen analysed by enzyme-linked immunosorbent assay. Antigen presentation was blocked by addition of anti-MHC class II monoclonal antibodies. GM, cortical grey matter. Data are mean + s.e.m., $n = 3$. One-way ANOVA. $*P < 0.05$, $**P < 0.01$. **d**, Interference with $T_{β\text{-syn}}$ cell activation prevents clinical disease. Disease course of rats that received $T_{β\text{-syn}}$ cells treated at the indicated time points (arrows) with either anti-MHC class II monoclonal antibodies (top) or FK506 (bottom). Vehicle-treated rats were used as control. Data are mean + s.e.m., $n = 10$ rats for anti-MHCII antibody and $n = 8$ rats for FK506 experiments. Unpaired two-tailed t-test. $*P < 0.05$, $**P < 0.01$, $***P < 0.001$.

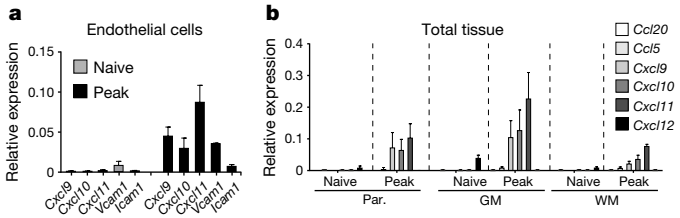

Fig. 4 | Antigenic activation of $T_{β\text{-syn}}$ cells induces an inflammatory reaction of CNS tissue. Upregulation of chemokines and integrins was determined by quantitative PCR. **a**, Expression of the indicated chemokine and integrin ligands in endothelial cells sorted from naive and diseased brain tissue at the peak of disease. **b**, Expression of the indicated chemokines in whole-brain tissue or from dissected cortex (grey matter) and corpus callosum (white matter (WM)). Data are mean + s.e.m., $n = 3$ rats, representative data of 2 independent experiments are shown.

with activated microglia and astrocytes after repeated bouts (Fig. 5d, e and Extended Data Fig. 9f). Moreover, clear signs of structural neuronal damage, such as destruction of the regular architecture of neurons and their processes, could be observed (Extended Data Fig. 9g). In fact, quantitative analyses revealed significant atrophy of the cortical tissue (Fig. 5f and Extended Data Fig. 9h). This permanent damage of the grey matter was confirmed using longitudinal MRI studies that demonstrated significant thinning of the brain cortex and enlargement of the ventricles. MRI analyses also revealed the dynamics of the atrophic process that had already started after the first bout, but which were significantly increased after consecutive attacks (Fig. 5g and Extended Data Fig. 9i–k).

β-Synuclein reactivity in patients with MS

Myelin-reactive T cells are known to be part of the immune repertoire of healthy people and are increased in patients with MS[21–24]. Studying the blood of healthy subjects, we found both MBP- and β-synuclein-reactive T cells. In patients with MS, the frequency of both cell specificities was higher (Fig. 6 and Extended Data Fig. 10a). As described previously for potentially auto-aggressive T cells[25–27], MBP- and β-synuclein-reactive T cells upregulated ICOS and CD25, expressed the CXCR3 and CCR6 chemokine receptors and produced proinflammatory cytokines, such as IFNγ and, to a lesser extent, IL-17 (Extended Data Fig. 10b–e). Notably, the frequency of β-synuclein-specific T cells was especially increased in patients with chronic-progressive MS, whereas the frequency of MBP-specific T cells was mainly increased in patients with relapsing-remitting MS (Fig. 6). The frequency of β-synuclein-specific T cells correlated with disease severity and duration (Extended Data Fig. 10f, g). Recently, α-synuclein-reactive T cells have been reported to be increased in patients with Parkinson's disease[28]. We confirmed the increased frequency of α-synuclein-reactive T cells in patients with Parkinson's disease, whereas β-synuclein-reactive T cells were not overrepresented in the blood of these patients. In patients with MS, the numbers of not only β-synuclein-specific T cells but also α-synuclein-specific T cells were increased (Fig. 6).

Our β-synuclein model makes it possible to study autoimmune processes that are directed against the complex and vulnerable grey matter, which distinguishes it from classic EAE models that affect only the 'wiring' and therefore the transmission of signals. The inability of EAE models to reflect grey matter pathology has generated speculation that alternative pathological mechanisms such as hypoxia or currently undefined soluble toxic factors initiate the degenerative grey matter process in MS[29]. Our data show that inflammation not only in white matter but also in grey matter can be induced by a targeted T-cell-driven attack. Antigen expression within the CNS and the specificity of T cells were crucial factors that determined the CNS target structures—not, as previously hypothesized, a special set of cytokines or adhesion molecules, or gravity[12–15,30]. Activation-induced release of cytokines by the T cells triggered a glial and vascular reaction that resulted in the formation of inflammatory lesions in the grey matter. It remains to be further clarified why it is that immunity against β-synuclein but not any of the other previously tested neuronal antigens, such as neurofilament or contactin-2[31,32], induces this overt, severe grey matter disease. Apart from a genetically encoded susceptibility—for example, the presence of certain MHC haplotypes that regulate the presentation capacity of antigenic peptides—the high expression levels of β-synuclein might have a conducing role. Furthermore, the association of β-synuclein with synapses and released vesicles—structures that have a high turnover within the CNS and as a consequence are in the reach of brain resident APCs—should render this neuronal autoantigen particularly recognizable by autoreactive T cells[33]. The tendency of synucleins to form aggregates[34] may be another contributing factor. Notably, β-synuclein-specific T cells not only cause inflammation but also induce significant chronic glial activation and neurodegeneration, particularly after repeated inflammatory bouts. The extent to which glial activation and/or inflammatory factors, such as cytokines, or the disruption of the BBB participate in the neurodegenerative process remains to be elucidated[1,35–37]. The neurodestructive component of our model reflects well the situation in MS, in which destruction of the grey matter is a hallmark of the disease—in particular, in the case of longstanding disabling MS[4]. Indeed, we found that β-synuclein-specific T cells were mainly increased in patients with chronic-progressive MS. Myelin-reactive T cells were predominant in patients with relapsing-remitting MS. This distinct chronological preponderance of the cell specificities could indicate that the β-synuclein-reactive T cells arise secondarily to the myelin-reactive T cells (for example, in the process of epitope spreading)[38]. However, β-synuclein-specific T cells were also detectable early in the

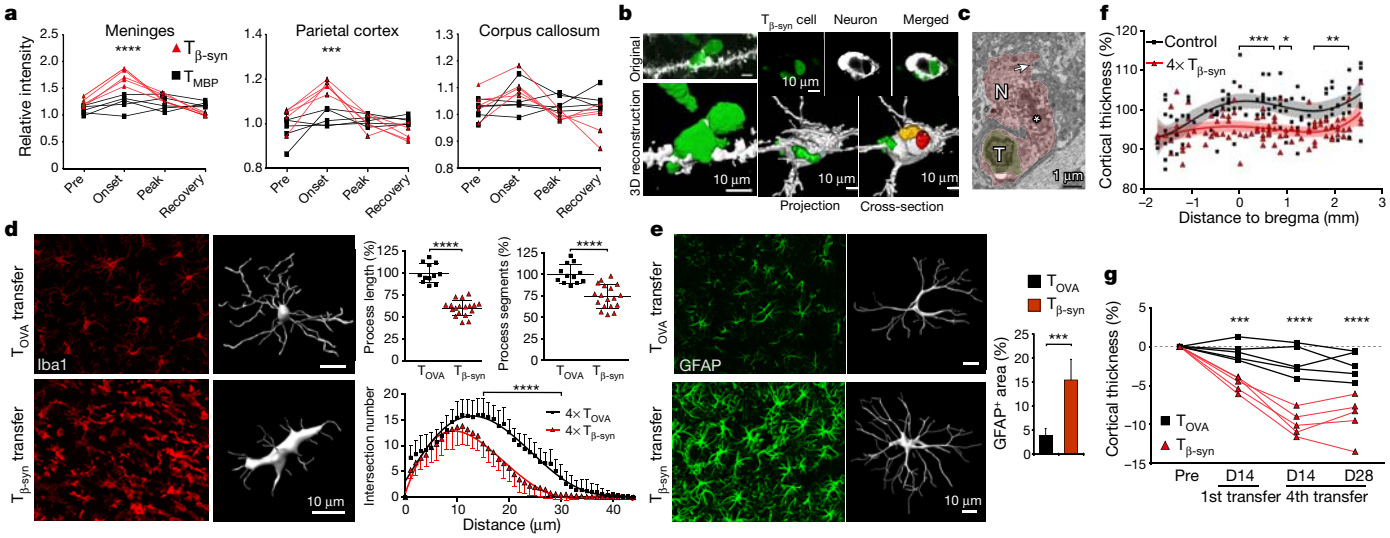

Fig. 5 | $T_{\beta\text{-syn}}$ cells induce grey matter damage. a, Quantification of Gd-enhanced MRI signals. Each line represents an individual rat. Representative data of two independent experiments are shown. $n = 5$ rats per group per experiment. Two-way ANOVA with Bonferroni's multiple comparison correction. **b**, **c**, $T_{\beta\text{-syn}}$ cells in close contact with neurons. **b**, Left, 3D-rendered confocal images depicting a $T_{\beta\text{-syn}}$ cell (green) in intimate contact with dendritic spines (white). Right, 3D reconstruction of $T_{\beta\text{-syn}}$ cells in contact (green) or partially or entirely engulfed (yellow and red, respectively) by a neuron (white). **c**, Electron microscopy image of a T cell (T) inside a neuron (N) with a fragmented and partly dissolved nucleus (asterisk). Arrow, synaptic terminal. **d**, **e**, $T_{\beta\text{-syn}}$ cell attacks induce persistent activation of microglia and astrogliosis. **d**, IBA1$^+$ microglia in the cortical grey matter after four consecutive transfers (4×) of T_{OVA} or $T_{\beta\text{-syn}}$ cells. Samples were collected three weeks after recovery from the last disease bout. Greyscale images, 3D reconstructions. Plots, quantification of process length and segments (unpaired two-tailed *t*-test) and number of intersections (two-way ANOVA with Sidak correction for multiple comparisons). Data are mean ± s.d. In total, 12 (4× T_{OVA}) and 18 (4× $T_{\beta\text{-syn}}$) cells per group were analysed obtained from 2 different rats from 2 sets of experiments per group. **e**, Representative confocal images and 3D reconstructions of GFAP$^+$ astrocytes. Plot, corresponding quantification of the morphological changes, pixels per area covered by GFAP staining. Data are mean + s.e.m., $n = 3$ rats per group, unpaired two-tailed *t*-test. **f**, **g**, $T_{\beta\text{-syn}}$ cell attacks induce cortical atrophy. **f**, Histological quantification of cortical thickness in control (age-matched naive and 4× T_{OVA}-cell-transferred rats) and 4× $T_{\beta\text{-syn}}$-cell-transferred rats. Mean cortical thickness of all controls over the entire anterior–posterior interval was set to 100%. Each dot represents mean thickness for a single rat at the indicated distance to bregma. Lines represent fitting curves (shading, 95% confidence interval) for the respective group of rats. $n = 9$ rats from 3 experiments for control, $n = 4$ rats from 4 experiments for 4× $T_{\beta\text{-syn}}$ cells. Unpaired two-tailed *t*-test. **g**, Longitudinal MRI measurements of the cortical thickness after 4× T_{OVA} or $T_{\beta\text{-syn}}$ cell transfer. Representative data of two independent experiments. $n = 5$ rats per group per experiment. Two-way ANOVA with Bonferroni's multiple comparison correction. **a**–**h**, $^*P < 0.05$, $^{**}P < 0.01$, $^{***}P < 0.001$, $^{****}P < 0.0001$.

disease process of cases with relapsing-remitting MS. Furthermore, inflammatory grey matter lesions were also observed early in MS[2]. A grey matter attack by neuronal antigen-reactive T cells might therefore be present from the very beginning of the autoimmune process and the accumulating irreversible neurological deficits of patients with chronic MS might be due to an exhaustion of the functional reserve, not necessarily because of epitope spreading. Clearly, future studies are needed to provide more insights into when β-synuclein-specific T cells expand, the functional role of these cells and how different treatments influence their functionality. In summary, our autoimmune grey matter inflammation model lends itself to the study of autoimmunity-mediated neurodegeneration and may open new avenues for the development of individual prognostic profiles and therapeutic measures for patients with MS.

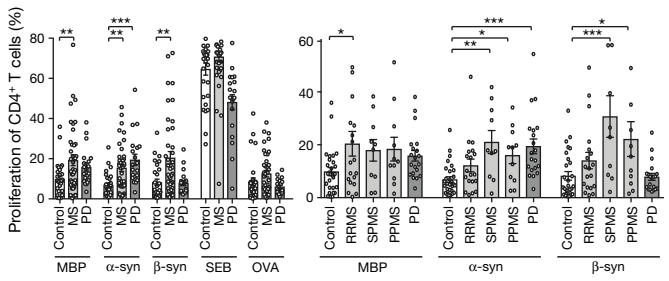

Fig. 6 | T cells reactive to β-synuclein are enriched in the blood of patients with MS. Left, percentage of proliferating CD3$^+$CD4$^+$ T cells of healthy subjects (control), patients with MS and patients with Parkinson's disease (PD) upon stimulation with the indicated antigens or SEB (*Staphylococcus* enterotoxin B). Right, T cell reactivity to β-synuclein is increased in patients with chronic MS. Percentages of proliferating CD3$^+$CD4$^+$ T cells in healthy subjects, patients with relapsing remitting MS (RRMS), secondary progressive MS (SPMS), primary progressive MS (PPMS) and patients with Parkinson's disease upon stimulation with the indicated antigens. Data are mean + s.e.m. One-way ANOVA with Dunnett's correction for multiple comparisons. $^*P < 0.05$, $^{**}P < 0.01$, $^{***}P < 0.001$.

Online content

Any methods, additional references, Nature Research reporting summaries, source data, statements of data availability and associated accession codes are available at https://doi.org/10.1038/s41586-019-0964-2.

Received: 6 August 2018; Accepted: 15 January 2019;
Published online 20 February 2019.

1. Peterson, J. W., Bö, L., Mörk, S., Chang, A. & Trapp, B. D. Transected neurites, apoptotic neurons, and reduced inflammation in cortical multiple sclerosis lesions. *Ann. Neurol.* **50**, 389–400 (2001).
2. Lucchinetti, C. F. et al. Inflammatory cortical demyelination in early multiple sclerosis. *N. Engl. J. Med.* **365**, 2188–2197 (2011).
3. Trapp, B. D. et al. Cortical neuronal densities and cerebral white matter demyelination in multiple sclerosis: a retrospective study. *Lancet Neurol.* **17**, 870–884 (2018).
4. Calabrese, M. et al. Exploring the origins of grey matter damage in multiple sclerosis. *Nat. Rev. Neurosci.* **16**, 147–158 (2015).
5. Wekerle, H., Kojima, K., Lannes-Vieira, J., Lassmann, H. & Linington, C. Animal models. *Ann. Neurol.* **36**, S47–S53 (1994).
6. George, J. M. The synucleins. *Genome Biol.* **3**, reviews3002.1 (2002).
7. Mor, F., Quintana, F., Mimran, A. & Cohen, I. R. Autoimmune encephalomyelitis and uveitis induced by T cell immunity to self β-synuclein. *J. Immunol.* **170**, 628–634 (2003).
8. Flügel, A. et al. Migratory activity and functional changes of green fluorescent effector cells before and during experimental autoimmune encephalomyelitis. *Immunity* **14**, 547–560 (2001).

9. Ben-Nun, A., Wekerle, H. & Cohen, I. R. The rapid isolation of clonable antigen-specific T lymphocyte lines capable of mediating autoimmune encephalomyelitis. *Eur. J. Immunol.* **11**, 195–199 (1981).
10. Odoardi, F. et al. T cells become licensed in the lung to enter the central nervous system. *Nature* **488**, 675–679 (2012).
11. Bartholomäus, I. et al. Effector T cell interactions with meningeal vascular structures in nascent autoimmune CNS lesions. *Nature* **462**, 94–98 (2009).
12. Reboldi, A. et al. C-C chemokine receptor 6-regulated entry of T_H-17 cells into the CNS through the choroid plexus is required for the initiation of EAE. *Nat. Immunol.* **10**, 514–523 (2009).
13. Rothhammer, V. et al. Th17 lymphocytes traffic to the central nervous system independently of α4 integrin expression during EAE. *J. Exp. Med.* **208**, 2465–2476 (2011).
14. Stromnes, I. M., Cerretti, L. M., Liggitt, D., Harris, R. A. & Goverman, J. M. Differential regulation of central nervous system autoimmunity by T_H1 and T_H17 cells. *Nat. Med.* **14**, 337–342 (2008).
15. Kroenke, M. A., Carlson, T. J., Andjelkovic, A. V. & Segal, B. M. IL-12- and IL-23-modulated T cells induce distinct types of EAE based on histology, CNS chemokine profile, and response to cytokine inhibition. *J. Exp. Med.* **205**, 1535–1541 (2008).
16. Li, J.-Y., Henning Jensen, P. & Dahlström, A. Differential localization of α-, β- and γ-synucleins in the rat CNS. *Neuroscience* **113**, 463–478 (2002).
17. Lodygin, D. et al. A combination of fluorescent NFAT and H2B sensors uncovers dynamics of T cell activation in real time during CNS autoimmunity. *Nat. Med.* **19**, 784–790 (2013).
18. Macian, F. NFAT proteins: key regulators of T-cell development and function. *Nat. Rev. Immunol.* **5**, 472–484 (2005).
19. Flügel, A. et al. Neuronal FasL induces cell death of encephalitogenic T lymphocytes. *Brain Pathol.* **10**, 353–364 (2000).
20. Ng, Y.-K. & Ling, E.-A. Emperipolesis of lymphoid cells in vagal efferent neurons following an intraneural injection of ricin into the vagus nerve in rats. *Neurosci. Lett.* **270**, 153–156 (1999).
21. Pette, M. et al. Myelin autoreactivity in multiple sclerosis: recognition of myelin basic protein in the context of HLA-DR2 products by T lymphocytes of multiple-sclerosis patients and healthy donors. *Proc. Natl Acad. Sci. USA* **87**, 7968–7972 (1990).
22. Ota, K. et al. T-cell recognition of an immunodominant myelin basic protein epitope in multiple sclerosis. *Nature* **346**, 183–187 (1990).
23. Bahbouhi, B. et al. T cell recognition of self-antigen presenting cells by protein transfer assay reveals a high frequency of anti-myelin T cells in multiple sclerosis. *Brain* **133**, 1622–1636 (2010).
24. Elong Ngono, A. et al. Frequency of circulating autoreactive T cells committed to myelin determinants in relapsing-remitting multiple sclerosis patients. *Clin. Immunol.* **144**, 117–126 (2012).
25. Latorre, D. et al. T cells in patients with narcolepsy target self-antigens of hypocretin neurons. *Nature* **562**, 63–68 (2018).
26. Cao, Y. et al. Functional inflammatory profiles distinguish myelin-reactive T cells from patients with multiple sclerosis. *Sci. Transl. Med.* **7**, 287ra74 (2015).
27. Jelcic, I. et al. Memory B cells activate brain-homing, autoreactive $CD4^+$ T cells in multiple sclerosis. *Cell* **175**, 85–100 (2018).
28. Sulzer, D. et al. T cells from patients with Parkinson's disease recognize α-synuclein peptides. *Nature* **546**, 656–661 (2017).
29. Lassmann, H. Multiple sclerosis pathology. *Cold Spring Harb. Perspect. Med.* **8**, a028936 (2018).
30. Arima, Y. et al. Regional neural activation defines a gateway for autoreactive T cells to cross the blood–brain barrier. *Cell* **148**, 447–457 (2012).
31. Krishnamoorthy, G. et al. Myelin-specific T cells also recognize neuronal autoantigen in a transgenic mouse model of multiple sclerosis. *Nat. Med.* **15**, 626–632 (2009).
32. Derfuss, T. et al. Contactin-2/TAG-1-directed autoimmunity is identified in multiple sclerosis patients and mediates gray matter pathology in animals. *Proc. Natl Acad. Sci. USA* **106**, 8302–8307 (2009).
33. Shibayama-Imazu, T. et al. Cell and tissue distribution and developmental change of neuron specific 14 kDa protein (phosphoneuroprotein 14). *Brain Res.* **622**, 17–25 (1993).
34. Taschenberger, G. et al. β-Synuclein aggregates and induces neurodegeneration in dopaminergic neurons. *Ann. Neurol.* **74**, 109–118 (2013).
35. Liddelow, S. A. et al. Neurotoxic reactive astrocytes are induced by activated microglia. *Nature* **541**, 481–487 (2017).
36. Petersen, M. A., Ryu, J. K. & Akassoglou, K. Fibrinogen in neurological diseases: mechanisms, imaging and therapeutics. *Nat. Rev. Neurosci.* **19**, 283–301 (2018).
37. Di Liberto, G. et al. Neurons under T cell attack coordinate phagocyte-mediated synaptic stripping. *Cell* **175**, 458–471 (2018).
38. Tuohy, V. K., Yu, M., Weinstock-Guttman, B. & Kinkel, R. P. Diversity and plasticity of self recognition during the development of multiple sclerosis. *J. Clin. Invest.* **99**, 1682–1690 (1997).

Acknowledgements We thank A. Stas, S. Mole, A. Mönnich, S. Hamann, M. Weig and H. Nguyen for technical assistance, C. Ludwig for text editing, G. Salinas-Riester for her support in performing the transcriptome analyses, K. Raithatha for her help in analysing the transcriptome data, H. Abken, S. Brioschi, L. Flügel, T. Issekutz, P. and W. von der Meide, M. Simons, T. Michaelis and M. Korte for providing reagents and/or technical, scientific or clinical advice and M. Gößwein for help with the artwork. This work was supported by the German Research Foundation (RK-Grant FL 377/3-1, FL 377/2-2; SFB 1328/1 A01, OD 87/1-1), the Federal Ministry for Education and Research (Competence Network Multiple Sclerosis, KKNMS), ERANET consortium MELTRA-BBB and the Ministry of Science and Culture of Lower Saxony (Niedersachsen-Research Network on Neuroinfectiology, N-RENNT).

Author contributions D.L. designed and cloned the TCR genes for the TCR transgenic rat and analysed the transgenic model. M. Hermann performed most two-photon laser-scanning microscopy experiments and, together with T.W., performed MRI. N.S. collected and analysed the human samples. C.F.-K. with the support of H.K. performed most of the morphological analyses. C. Schlosser analysed the initial grey matter disease model. A.M. performed transcriptome and functional analyses. H.-F.C. established the CAR system. H.J.F. performed oocyte injections. H.M.R. contributed his expertise in rat transgenesis, M.Z. helped to analyse neurodegeneration and B.M. recruited patients with PD. S.K. provided the AAVs. D.F. collected samples from patients with MS. J.F. helped with providing and optimizing MRI technology, C. Stadelmann provided advice on CNS pathology and M. Haberl helped to analyse the NGS data. F.O. performed most of the ex vivo T cell and APC analyses. A.F. together with F.O. designed the study, coordinated the experimental work and wrote the manuscript with inputs from co-authors.

Competing interests The authors declare no competing interests.

Additional information

Extended data is available for this paper at https://doi.org/10.1038/s41586-019-0964-2.
Supplementary information is available for this paper at https://doi.org/10.1038/s41586-019-0964-2.
Reprints and permissions information is available at http://www.nature.com/reprints.
Correspondence and requests for materials should be addressed to F.O. or A.F.
Publisher's note: Springer Nature remains neutral with regard to jurisdictional claims in published maps and institutional affiliations.

METHODS

Wild-type rats. Lewis rats on a LEW/Crl background (*Rattus norvegicus*) were bred at the animal facility of the University Medical Center Göttingen (Germany). The rats were kept under standardized conditions on a 12-h light–dark cycle. They were provided with food and drink ad libitum. All experiments were performed according to the local animal welfare regulations. Both male and female rats were used in the EAE experiments. No differences were noted between the sexes.

Generation of transgenic rats. Wild-type Lewis rats were immunized with rat β-synuclein protein (Creative BioMart). After 10 days, lymph node cells were isolated and amplified by exposing them to β-synuclein (10 μg ml^{-1}). Seven days later, lymphocytes were rechallenged using a β-synuclein peptide library covering the entire protein sequence. The peptides β-syn$_{79–98}$ and β-syn$_{93–111}$ gave the most pronounced proliferative response (Extended Data Fig. 1a). β-Syn$_{93–111}$ was then selected for further testing and for the generation of transgenic rats. The generation of β-synuclein-specific TCR-transgenic Lewis rats and their detailed characterization will be described elsewhere (L.D., manuscript in preparation). In brief, clonal effector T cell lines established from immunized Lewis rats were used to determine the sequence of rearranged α and β TCR chains that confer specificity to rat β-syn$_{93–111}$. These sequences were fused as a tricistronic eGFP-T2A-TCRα-P2A-TCRβ cassette, which was cloned into the self-inactivating lentiviral vector FUGW by replacing the GFP insert. Gene transfer was performed by microinjection of concentrated viral particles into the perivitelline space of fertilized Lewis oocytes (donors obtained from Charles River) as previously described[39]. Founder rats were identified by genomic PCR of skin biopsies and flow cytometry analysis of blood samples. Rats were bred to homozygosity and maintained for several generations under standard conditions.

Antigens. MBP was extracted from guinea pig brain as described[40], OVA was purchased from Sigma, recombinant rat β-synuclein was purchased from Creative BioMart or purified in-house from bacterial *E. coli* lysates expressing recombinant protein with C-terminal 6×His tag using a Ni-agarose column. All peptides were synthetized by the peptide facility of the Charité (Berlin).

Generation and culturing of T cells. CD4$^+$ T cells retrovirally engineered to express fluorescent proteins (eGFP, mCherry, TdTomato, Turquoise2 or LifeAct-Turquoise2) or NFAT reporter (NFAT–YFP or NFAT–YFP/Cherry-H2B) and reactive against β-syn$_{93–111}$, MBP or OVA ($T_{β\text{-syn}}$, T_{MBP} or T_{OVA} cells) were established as reported[17,41]. For the generation of chimeric antigen receptor-expressing T cell lines (CAR T cells), the sequence encoding SCA431scFv-mIgG1-CD4tm-CD3ζ CAR specific for carcinoembryonic antigen[42] (courtesy of H. Abken, University of Cologne) was excised from the pBullet vector and cloned into a pMSCV-Puro-P2A vector, which was then used to establish a stable retroviral packaging cell line. The mouse single-chain antibody domain of CAR was used to activate CAR T cells in situ by application of crosslinking anti-IgG1 monoclonal antibodies.

In brief, 6–8-week-old female Lewis rats were immunized subcutaneously with 150 μl of emulsion prepared from β-syn$_{93–111}$, MBP or OVA (stock concentration: 1 mg ml^{-1}) and an equal volume of complete Freund's adjuvant containing *Mycobacterium tuberculosis* extract (Difco) at a concentration of 2 mg ml^{-1}. The cell suspension isolated from the draining lymph nodes 9–10 days after immunization was co-cultured with GP+E86 packaging cell lines producing replication-deficient retroviruses in the presence of 10 μg ml^{-1} MBP or OVA or 8 μg ml^{-1} of β-syn$_{93–111}$. After 48 h, medium containing horse serum (10%, Biochrom AG) and mouse IL-2 was added to the culture for T cell expansion. Starting from day 4 after antigen stimulation, transduced T cells were selected by the addition of G418 (400 mg ml^{-1}, Thermo Fisher) for two weeks or puromycin (1 μg ml^{-1}, Carl Roth) for one week. Seven days after primary stimulation, T cells were rechallenged with the cognate antigen in the presence of 30-Gy-irradiated thymic APCs. The primary cell lines underwent at least three cycles of stimulation in culture before being used for transfer experiments. For the derivation of transgenic T cell lines, lymph node cells were explanted six days after immunization and antigen restimulation was performed every six days. All established T cell lines were CD4$^+$CD8$^-$αβTCR$^+$. They displayed an effector memory phenotype (L-selectin$^-$CD45RC^{low}CD44^{high}) and upon stimulation produced IFNγ and IL-17. Phenotype, cytokine profile, antigen specificity, pathogenicity and the absence of mycoplasma contamination were verified in each cell line.

In vitro activation assays were performed in 96-well plates by co-culturing 5×10^4 T cells and 10^6 30-Gy-irradiated thymocytes per well. For unspecific stimulation, T cells were added onto plates coated with anti-CD3 (1 μg ml^{-1}, clone G4.18, BD Biosciences) and anti-CD28 (2 μg ml^{-1}, clone JJ316, BD Biosciences) monoclonal antibodies or treated with 2 μg ml^{-1} concanavalin A (Sigma). For blocking MHC class II-mediated antigen presentation, APCs were pretreated with 1 μg ml^{-1} anti-RT1b monoclonal antibodies (clone OX-6, Biolegend) before being added to T cells.

Transfer EAE. Adoptive transfer EAE was induced by intravenous injection of T cell blasts (day 2 after stimulation). Unless stated differently, the following number of T cells were injected: 7–8 × 10^6 wild-type $T_{β\text{-syn}}$ cells, 2–3 × 10^6 transgenic $T_{β\text{-syn}}$ cells or 5 × 10^6 T_{MBP} cells. For T_{OVA}-cell transfer, 5 × 10^6 cells were injected. In cotransfer experiments, equal numbers (3–4×10^6) of $T_{OVA–Tomato}$ and $T_{β\text{-syn–Turquoise}}$ cells were injected intravenously into naive recipients.

Relapsing-remitting EAE was induced by repeated transfer of 2.5 × 10^6 transgenic $T_{β\text{-syn}}$ or T_{MBP} cell blasts into TCR-transgenic rats. After each transfer, the rats developed a severe monophasic disease with comparable severity of disease symptoms. β-Synuclein transgenic animals repeatedly injected with T_{OVA} cells (5 × 10^6 cells per rat) were used as control. As expected, upon repeated transfer of transgenic $T_{β\text{-syn}}$ cell blasts, wild-type rats became completely resistant to disease induction[33].

Weight and clinical scores were recorded daily. Classical signs of EAE were scored as follows: 0, no disease; 1, flaccid tail; 2, gait disturbance; 3, complete hindlimb paralysis; 4, tetraparesis; 5, death. For atypical symptoms, the following classification was used: 0, no disease; 1, occasional twitches and scratching with or without flaccid tail; 2, frequent twitches and scratching, ataxia; 3, severe tonic and myoclonic movements, severe gait impairment; 4, tetraparesis; 5, death.

No statistical method was used to predetermine sample size. Rats from different cages but within the same experimental group were selected to assure randomization. Experimenters were blinded to the identity of experimental group in the experiments as follows: clinical effect of cytokine blockers; morphological analysis; acquisition and analysis of the human samples.

Cell isolation, flow cytometry and fluorescence-activated cell sorting. Fluorescently labelled T cells were isolated from the tissues as previously described[8,10]. In brief, mononuclear cells were isolated from EDTA-treated blood by density gradient. Single-cell suspensions were obtained from parenchymal organs, grinding the tissues through a mesh. The isolated cells underwent different procedures: spleen-derived single-cell suspensions were treated with ACK buffer for erythrocyte lysis. Immune cells were extracted from the different CNS compartments by a two-phase Percoll-density gradient. Isolation of CD11b$^+$ microglial cells was performed as described[43]. In brief, rats were perfused with saline, meninges were removed and grey matter was isolated under a stereotactic microscope. CD11b$^+$ microglial cells were then isolated with a three-phase Percoll-density gradient. Of note, no enzymatic digestion of the tissue was performed.

For the isolation of endothelial cells, euthanized rats were transcardially perfused with ice-cold PBS. Brain tissue was dissected and meninges were removed. The parenchyma was homogenized in a Dounce tissue grinder before the tissue was digested for 1 h in digestion buffer (HEPES-buffered DMEM medium supplemented with 0.4 U ml^{-1} liberase (Roche), 120 U ml^{-1} DNase I (Roche)) at 37 °C. Digestion was stopped by adding ice-cold buffer with 2 mM EDTA and samples were passed through a 20G syringe and filtered through a 70-μm cell strainer. Myelin debris was removed by 30% Percoll gradient centrifugation for 20 min at 700*g*. Cells were stained in staining buffer (PBS with 2 mM EDTA and 0.5% BSA) with anti-CD31–PE antibodies (Bio-Rad, clone TLD-3A12, dilution 1:100), anti-CD45–AF647 (Biolegend, clone OX-1, dilution 1:100) and anti-CD11b–AF647 (Biolegend, clone OX-42, dilution 1:100) for 30 min at 4 °C, washed twice with staining buffer then resuspended in HEPES-buffered DMEM with 2 mM EDTA for fluorescence-activated cell sorting (FACS). Labelled cell populations were sorted by a FACSAria 4L SORP cell sorter (Becton Dickinson). Sorted cells were pelleted for 5 min at 300*g* and taken up in QIAzol Lysis Reagent (Qiagen) for RNA isolation.

Flow cytometry analysis was performed with a FACSCalibur operated by Cell Quest software (Becton Dickinson) or by a CytoFLEX flow cytometer operated by CytExpert software (v.2.3, Beckmann Coulter). All procedures were performed at 4 °C. For surface staining, the following mouse anti-rat monoclonal antibodies were used: CD134–biotin (clone OX-40, Serotec), CD25–PE (clone OX-39, Biolegend), CD11b/c–AF647 (clone OX-42, Biolegend), αβTCR–AF647 or αβTCR–PE (clone R73, Biolegend), TCR Vβ8.2 (clone R78, Santa Cruz Biotechnology), TCR Vβ8.3 (clone B73, Serotec, described to recognize Vβ8.5[44], but it actually recognized Vβ8.3 as described[45]), TCR Vβ10 (clone G101, Serotec), TCR Vβ16.1 (clone His42, Serotec), γδTCR–PE (clone V65, Biolegend), CD45–PE (clone OX-1, Biolegend), CD45RA–PE (clone OX-33, Biolegend), CD8α–PE (OX-8, Biolegend), CD8β-PE (clone eBio341, eBioscience), CD3–AlexaFluor647 (clone 1F4, Biolegend), CD4–PECy5 (clone W3/25, BD Biosciences), CD4–PE–Cy7 (clone OX-35, BD Biosciences), CD28–APC (clone JJ319, Biolegend), CD62L–PE (clone OX-85, Biolegend), CD45RC–PerCP–Cy5.5 (clone OX-22, Abcam). Mouse IgG1κ (MOPC 31C, Sigma-Aldrich) served as isotype control; APC-labelled anti-mouse antibody (Dianova) was used as secondary antibody. For intracellular staining, mouse anti-rat IFNγ (DB-1, conjugated to AF647, Biolegend), rat anti-mouse IL-17–BV421 (clone TC11-8H4, Biolegend) and anti-Ki-67–AF647 (clone B56, BD Biosciences) antibodies were used. Before staining, cells were fixed and permeabilized using a BD Cytofix/Cytoperm kit (BD Biosciences) as recommended by the manufacturer. Mouse IgG1κ–AF647 (clone MOPC21, Biolegend) and rat IgG1κ–BV421 (clone RTK2071, Biolegend) antibodies were used as control. For the analysis of human peripheral blood mononuclear cell (PBMC) cultures the following antibodies

were used: CD3–APC or CD3–APCFire750 (clone UCHT1, Biolegend), CD4–PE (clone RPA-T4, Biolegend), CD8–PECy5 (clone RPA-T8, Biolegend), CD25–PE–Cy5 (clone BC96, Biolegend), ICOS–PacificBlue (clone C398.4A, Biolegend). Cytofluorometric quantification of T cells was performed by relating the number of cells to a known absolute amount of fluorescent beads (BD Biosciences). Data analysis was performed using FlowJo software (FlowJo).

Cell proliferation analysis using BrdU incorporation assay. BrdU incorporation was measured as previously reported[11]. In brief, for ex vivo analysis BrdU (120 mg kg^{-1} body weight, Sigma-Aldrich) was injected intraperitoneally 2 h before organ collection. This time interval between BrdU injection and sample collection was chosen to minimize cell trafficking and to allow BrdU to enter the CNS parenchyma. For in vitro labelling, T cells were incubated with 10 μM BrdU for 2 h. Intracellular staining for BrdU was then performed using the BrdU APC Flow kit (BD Biosciences) according to the manufacturer's instructions. The T cells were then analysed by flow cytometry.

Intravital two-photon laser-scanning microscopy. *Surgical procedures.* Two-photon laser-scanning microscopy (TPLSM) was used for imaging fluorescently labelled T cells in the brain of living rats. Imaging was performed in the preclinical phase and at the onset and peak of the disease. For this purpose, rats were pre-anaesthetized by intramuscular injection of 10 mg kg^{-1} xylazine combined with 50 mg kg^{-1} ketamine and then intubated via a small incision of the trachea and immediately ventilated with 1.5–2% isoflurane. During imaging, rats were stabilized in a custom-made microscope stage and their body temperature regulated and maintained (36–37 °C) via a heated pad connected to a custom-built thermocontroller. Fluid supply during imaging sessions was maintained using a perfusing device (Ismatec) set to a 0.6 ml h^{-1} flow rate. To access the parietal cortex, an open-skull window preparation was performed. In brief, a midline scalp incision was performed to expose the parietal, interparietal and frontal bones. The skull was then stereotactically fixed with dental paste to a head holder. Subsequently, a microdrill was used to cut an ellipsoid area of around 0.5 cm^2 in the parietal bone (coordinates from bregma: $x = +1.5$ mm, $y = -1$ mm). The dura mater was carefully removed. For all preparations, tissue was immediately covered with sodium chloride solution to prevent dehydration.

Technical equipment and labelling procedures. TPLSM imaging was performed as previously described[46], using two different systems: (1) a Zeiss Laser Scanning Microscope 710 (Carl Zeiss) combined with a Coherent 10 W Ti:Sapphire chameleon laser (Coherent), controlled by Zeiss ZEN 2012 software; and (2) an Olympus FVMPE-RS TPLSM equipped with a Spectra-Physics Mai Tai Ti:Sapphire oscillator and a Mai Tai DeepSee Ti:Sapphire oscillator. The excitation wavelength was tuned to 880 nm or 1,010 nm and routed through a 20× water 1.0 NA immersion objective W Plan Apochromat (Carl Zeiss) and a 25× water 1.05 NA immersion objective Olympus Scaleview in the Zeiss and in the Olympus TPLSM, respectively. Farred fluorescent proteins (for example, TdTomato) were excited at 1,100 nm either using a Ti:Sapphire laser pumped OPO in the Zeiss TPLSM or a Mai Tai DeepSee Ti:Sapphire oscillator in the Olympus TPLSM. Emitted fluorescence was detected using non-descanned detectors equipped with 442/46 nm, 550/49 nm and 624/40 nm band-pass filters. Typically, areas of 424.27 μm × 424.27 μm (512 × 512 pixels) width were scanned and 50–100-μm *z*-stacks were acquired. The acquisition rate during bidirectional scanning was approximately 1.3 s per *z*-plane including 2 times line-averaging. For reproducible motility analyses, the interval time was kept to 30 s. Blood vessels were labelled by intravenous injection of 2,000,000 Da dextran tetramethylrhodamine (Fischer Scientific) during the imaging session. Meningeal phagocytes were labelled by intrathecal injection of 3,000 Da dextran Texas red (Fischer Scientific) 24 h before imaging. To label myeloid cells, a monoclonal antibody against CD11b (OX-42) labelled in-house with SeTau647 (SETA BioMedicals) was injected intrathecally immediately before imaging. For evaluating BBB permeability, 70,000 Da dextran Texas red (Fischer Scientific) was injected before imaging.

Analysis of time-lapse videos. Acquired 3D time-lapse videos were analysed using Imaris 8.0.1 software (Bitplane AG). Cells were tracked using the automated Imaris Track module with subsequent manual revision. Motility parameters including T cell velocity (instantaneous speed average), crawling duration and meandering index (total T cell path length/single-cell displacement sum) were calculated as described[46] within a 30-min recording interval. Rolling T cells were defined as cells appearing as single or several round-shaped dots with >50 μm min^{-1} instantaneous velocity. Owing to limitations in temporal resolution of the TPLSM, fast rolling events may have escaped our analysis.

In vivo integrin signal blockade. Integrin-mediated binding was blocked as previously described[11] using mouse anti-rat monoclonal antibodies directed either against VLA-4 (anti-CD49d, clone TA-2; courtesy of T. Issekutz, Dalhousie University, Canada) or against CD11a (integrin αL, anti-LFA-1, clone WT.1, Serotec). For intravital TPLSM recordings in the intravascular phase, monoclonal antibodies were injected intravenously at a single dose of 1 mg kg^{-1} during the imaging session. After recording, ex vivo isolated T cells were tested by flow cytometry for antibody saturation. For assessing the clinical effects monoclonal antibodies were administered intrathecally twice (40 μg per rat per injection), namely on day 2.5 and 3.5 after T cell transfer.

In vivo inflammatory cytokine blockade. IFNγ and IL-17 were blocked by anti-rat IFNγ (provided by W. van der Meide) and anti-rat IL-17A (provided by Novartis) monoclonal antibodies, respectively. Antibodies were injected intrathecally (80 μg per rat per injection) on day 1.5, 2.5 and 3.5 after T cell transfer. In a preliminary experiment, mouse IgG1 or PBS were used as control. Given that results were identical between the IgG1 and PBS groups, in all subsequent experiments, PBS was used as control.

In vitro antigen presentation. Microglial cells (5×10^4 per 100 μl) isolated as described above were cocultured with $T_{\beta\text{-syn}}$, T_{MBP} or T_{OVA} cells (3×10^4 per 100 μl for each cell line) in 96-well plates with or without the cognate antigen (10 μg ml^{-1}) and in the presence or absence of MHC-II blocking monoclonal antibodies (10 μg ml^{-1}). After 48 h, the cell culture supernatant was collected. Enzyme-linked immunosorbent assay (ELISA) assays were used to detect the concentrations of IFNγ and were carried out according to the manufacturer's protocol (PeproTech).

Chemotactic assays. A trans-well migration assay was used to test the chemotactic capacity of blood-isolated antigen-specific cells towards CCL5 (0.1 ng ml^{-1}), CCL19 (0.1 ng ml^{-1}), CCL20 (0.1 ng ml^{-1}), CXCL11 (0.1 ng ml^{-1}), CXCL12 (0.1 ng ml^{-1}) as described[47]. All chemokine ligands were purchased from Peprotech. The number of effector T cells migrating in response to the chemokine ligands was counted by flow cytometry and quantified in relation to the basic migration in the absence of chemokine ligands.

In vivo MHC class II blockade. MHC class II-mediated antigen presentation was blocked by intrathecal injection of anti-rat MHC class II monoclonal antibodies (80 μg per rat per injection) performed on days 1.5, 2.5 and 3.5 after T cell transfer.

FK506 treatment. FK506 (Sigma-Aldrich) was administered as previously described[17]. The drug was dissolved in DMSO (Carl Roth) to a concentration of 2 mg ml^{-1} and injected intraperitoneally at a dose of 2 mg kg^{-1} once per day. Control rats received an intraperitoneal injection of an equal volume of DMSO.

Activation of $T_{OVA\text{–}CAR}$ cells. In vitro activation of resting $T_{OVA\text{–}CAR}$ cells (day 6 after antigen challenge) was achieved by two different methods: (1) stimulation with increasing doses (0.5, 5, 50 μg ml^{-1}) of biotinylated anti-mouse IgG1 monoclonal antibodies (clone RMG1-1, BioLegend) with or without crosslinking streptavidin (0.5 μg ml^{-1}, Biolegend); and (2) stimulation with anti-rat CD3 (0.1 mg ml^{-1}, clone G4.18, BD Biosciences) and CD28 (0.5 mg ml^{-1}, clone JJ316, BD Biosciences) monoclonal antibodies, which had been coated on the culture plate before adding the T cells.

For in vivo activation, rats were injected with 10 μl anti-mouse IgG1 monoclonal antibody (50 μg ml^{-1}) 3 days after $T_{OVA\text{–}CAR}$ cell transfer. The monoclonal antibody was injected with a stereotactic devise (Narishige) either in the cisterna magna (intrathecally) or in the right ventricle (intracerebroventricular (i.c.v.); coordinates from bregma: $x = +1.5$ mm; $y = -1.0$ mm, $z = -4.3$ mm). The solution was injected at a rate of 10 μl in 5 min to limit increase in intracranial pressure. After 5 min, the needle was slowly retracted (1 mm every 5 min) to avoid reflow through the injection route. The two injection modes gave equivalent results and therefore the results were pooled.

In vivo delivery of soluble antigen. To boost antigen presentation, 3 days after transfer of T_{MBP} cells or T_{OVA} cells, rats were injected with MBP or OVA (10 μg per rat), respectively. The antigens were injected either intrathecally or i.c.v. as described above. The two injection modes gave equivalent results and therefore the results were pooled. TPLSM or FACS quantification was performed 12 h later.

Neuronal overexpression of β-synuclein. AAV vectors were constructed to express β-syn–eGFP, γ-syn–eGFP, or eGFP under the human synapsin promoter as previously described[48]. An AAV2 serotype was selected, because of its higher selectivity for neuronal cells. AAV vectors were injected intracranially into neonatal rats 24–48 h after birth. Each rat received 2 μl of solution containing 1.5×10^8 transducing units. Six weeks later, the rats were intravenously transferred with 2.5×10^6 $T_{\beta\text{-syn}}$ cells.

RNA extraction, cDNA library preparation and RNA sequencing. RNA extraction, cDNA library preparation and RNA sequencing (RNA-seq) was performed as described[47]. For T cell sequencing, total RNA from wild-type or transgenic $T_{\beta\text{-syn}}$ cells was isolated either from in vitro $T_{\beta\text{-syn}}$ cell blasts (20 h after antigen encounter) or ex vivo from blood, brain leptomeninges and brain parenchyma 3 days post transfer (p.t.). Between 200,000–400,000 $T_{\beta\text{-syn}}$ cells were sorted from each sample achieving more than 98% purity. Three different biological replicates were prepared for each sample. Four to five rats were pooled for each replicate. Library preparation for RNA-seq was performed using the TruSeq RNA Sample Preparation Kit (Illumina, RS–122–2002) starting from 500 ng of total RNA. Single-read (45-bp) sequencing was conducted using a HiSeq 2000 (Illumina). Sequences were aligned to the genome reference sequence of *R. norvegicus* allowing for 2 mismatches within 45 bases. Gene annotation was performed using

R. norvegicus entries from Ensembl v.78. Data of gene expression profiles of T_{MBP} cells were obtained from a previously published dataset[47].

Quantitative PCR. Quantitative PCR was performed on a StepOnePlus Real-Time PCR System (Applied Biosystems) using FAM-TAMRA-labelled probes as described[10,47]. *ACTB* was used as house-keeping gene. For detecting cytokine and chemokine expression on human samples the following primers/probe combination was used with *RPL13A* as house-keeping gene: *IFNG*: forward, TCTCTCGGAAACGATGAAATATACAA; reverse, TTTTACATATGGGTCC TGGCAGTA; probe, ATCTTGGCTTTTCAGCTCTGCATCGTTTTG. *IL17*: forward, TGTGATCTGGGAGGCAAAGT; reverse, CCCACGGACACCAGTA TCTT; probe, AGCCTCCCTGCGCAGGACCA. *IL4*: forward, GCCTGG CGGGCTTGA; reverse, AGCCTTTCCAAGAAGTTTTCCA; probe, CCTGTCCTGTGAAGGAAGCCAACCA. *CXCR3*: forward, CTATGACTA TGGAGAAAACGAGAGTGA; reverse, GGCCCGGTCGAAGTTCA; probe, TCGTGCTGTACCTCCCCGCCC. *CCR6*: forward, TTGTACAGGCGACTA AGTCATTCC; reverse, CCCACACAACAAGGCAGATG; probe, CTCCGA TCCAGAACACTACCGCGC. *RPL13A*: forward, CTGTGAAGGCATCAACA TTTCTG; reverse, TCGGGAAGGGTTGGTGTTC; probe, TTGAAGTACCTGG CTTTCCTCCGCAA

Magnetic resonance imaging. MRI was performed at 9.4 T. Radiofrequency excitation and signal reception were accomplished by a birdcage resonator and a four-channel phased-array surface coil, respectively (both from Bruker Biospin MRI). Multislice fast spin-echo MRI was used to perform T2-weighted axial MRI with repetition time (TR) of 9,286 ms, echo time (TE) of 11 ms, RARE factor of 12, 60 slices, in-plane resolution of 120 μm × 120 μm, slice thickness of 480 μm and a total acquisition time (TA) of 195 s. In addition sagittal MRI (TR/TE = 4,333/11 ms, RARE factor = 12, 28 slices, in-plane resolution = 120 μm × 60 μm, slice thickness of 480 μm and TA = 182 s) was performed. T1-weighted fat-suppressed gradient-echo MRI (3D FLASH, TR/TE = 14.8/4.2 ms, flip angle = 25° and TA = 16 min) was performed at an isotropic resolution of 120 μm before and after intravenous injection of 30 μl gadobutrol, a Gd-based contrast agent (stock concentration: 1 mM, Gadovist, Bayer). The analysis followed a strategy previously developed for intra-individual comparisons of MR images[49]. For quantifying Gd enhancement, MRI signal intensities were evaluated. For this purpose, regions of interest (ROIs) were selected in a standardized manner: the signal intensity in the meninges was calculated using mid-sagittal T1-weighted planes; for the analysis of signal intensities in parietal cortex, corpus callosum and thalamus, T1-weighted images 0.5 mm lateral from the mid-sagittal plane were used. The mean signal intensity was measured for all ROIs and normalized to the signal intensity of the thalamus. Subsequently, the ratio between normalized signal intensity before and after Gd injection was calculated. For measuring its thickness, the corpus callosum was marked in T2-weighted planes 0.5 mm lateral from the mid-sagittal section by two parallel lines. The distance between those lines was measured at both endpoints. For measuring cortical thickness, the distance between corpus callosum and meninges was measured at three points. The measurements were taken in both hemispheres and subsequently averaged. Ventricular size was assessed by 3D reconstruction of the third and lateral ventricles from T2-weighted images. All analyses were performed with Fiji software.

Analysis of neuronal synaptic spine density. Rats were transcardially perfused with ice-cold 1× PBS (2 min) and 4% PFA (10 min) at the peak of T cell infiltration. Hemispheres were then separated and post-fixed in 4% PFA for 30 min. One hemisphere was set aside for histology, the other embedded in 2–3% low-melt agarose (Roth) and cut into 300-μm thick slices on a vibratome (Leica VT1200S). Slices were washed three times 15 min in 1× PBS. Cortical neurons were analysed using DiOlistic labelling on acute slices as described[50]. In brief, DiI-coated tungsten particles (0.7 and 1.7 μm in diameter; Bio-Rad) were delivered to the slices using a hand-held gene gun (Helios Gene Gun System, Bio-Rad). After 48 h, images were acquired by confocal microscopy. Synaptic spines in apical dendrites from DiI-stained L2/3 pyramidal neurons were counted on deconvoluted images using Fiji software. The number of spines was normalized per micrometre of dendritic length.

Confocal microscopy. Confocal microscopy was performed using a Zeiss Laser Scanning Microscope 710 (Carl Zeiss) controlled by Zeiss ZEN 2012 software (Carl Zeiss) and a custom-made microscope that combines two-photon, confocal and stimulated emission depletion microscopy (Abberior instruments). Fluorophores were excited using 405-nm UV-diode for DAPI, 488-nm Argon laser for GFP, a 561-nm DPSS laser for mCherry or DiI and a 633-nm HeNe laser for Cy5 dyes. Accordingly, filters were set from 415 to 470 nm for DAPI acquisition, 498 to 546 nm for GFP and 571 to 660 nm for mCherry/DiI/Cy5. A 40× oil/1.3 NA immersion objective Plan Apochromat objective (Carl Zeiss) was used. Images were acquired using a pinhole size of 50 μm. A *z*-step size of 0.5 μm was chosen to guarantee optimal *z*-resolution. T cell quantification was performed on single *z*-stack using the cell-counter plug-in in ImageJ with manual corrections.

Histology and immunohistochemistry. Rats were intracardially perfused with saline (10 min) followed by a fixative containing 4% PFA (15 min). Samples were post-fixed in the same fixative for 24 h and then transferred in 30% sucrose. Histological analysis was performed according to established procedures on paraffin and frozen sections. The following antibodies were used: mouse anti-rat RT1B-MHC class II antigen (clone OX-6, Serotec), rabbit anti-IBA1 (Wako), mouse anti-rat CD68 (clone ED1, Serotec), mouse anti-neurofilament marker (Biolegend), mouse anti-GFAP (Thermo Fisher), mouse anti-rat CD43 (clone W3/13, Biolegend), rabbit anti-β-synuclein (AB 5086, Millipore), rabbit anti-tyrosine hydroxylase (Millipore) and goat anti-mouse or goat anti-rabbit IgG antibodies labelled with Alexa Fluor 488, Alexa Fluor 555 or Alexa Fluor 647 (Invitrogen) as secondary antibodies. Images were acquired using either a VS120 Virtual Slide Microscope (Olympus) equipped with a 10× objective or with a Zeiss LSM700 confocal microscope equipped with a 40× Zeiss objective. For morphological quantification, images of brain sections cut coronally in series were acquired with a BZ-9000 Keyance microscope. The total length of the cortex ranging from the corpus callosum to the meningeal surface was measured along the orientation of the neuronal processes (dendrites) in the motor region M1 using the BZ-9000 Keyance software. In addition, the corpus callosum was measured at its thickest site close to the midline. Morphological analysis and 3D reconstruction of microglia stained with anti-rat IBA1 and astrocytes stained with anti-rat GFAP were done using Imaris 8.0.1 software (Bitplane AG) as previously described[51]. Confocal *z*-stacks with 0.5-μm step size were opened in Imaris and smoothed with both median and Gaussian filters. Single cells were rendered by first using the filament tool to reconstruct the processes and subsequently the surface tool to render the cell body. Process length and number of segments (segments between branch points or branch and endpoints) were analysed.

Electron microscopy. Rats were intracardially perfused with saline followed by a fixative containing 4% PFA and 1% glutaraldehyde. After postfixation in Ito's solution and washing in cacodylate buffer, brain tissue was cut into 2 mm × 2 mm specimens. After postfixation in 1% osmium tetroxide, the specimens were dehydrated with graded alcohols and embedded in Epon (Roth). Then, 1-μm semi-thin sections were cut by a microtome (Reichert-Jung) and stained with Richardson's staining. Ultrathin sections were cut with an Ultracut E microtome (Reichert-Jung), contrasted with lead citrate and uranyl acetate and imaged with a Zeiss EM 109.

Patients and control donors. T cell assays were performed using PBMCs prepared from 29 healthy controls, 40 patients with MS and 20 patients with Parkinson's disease. Detailed clinical information is included in Extended Data Fig. 10a. This study was approved by the local ethical committee, and all patients gave their informed consent for the study.

Isolation of PBMCs, proliferation assay and CD3 stimulation. PBMCs isolated from human peripheral blood by Ficoll gradient were labelled with 5-chloromethylfluorescein diacetate (CFSE, Invitrogen) at a density of 1×10^6 cells per ml using 0.5 μM CFSE and cultured for 7 days in the presence of the following antigens: human β-synuclein (50 μg ml^{-1}, Abcam), human α-synuclein (50 μg ml^{-1}, provided by M. Zweckstetter, MPIBC, Germany), MBP (50 μg ml^{-1}), OVA (50 μg ml^{-1}, Sigma-Aldrich) or staphylococcal enterotoxin B (10 μg ml^{-1}, Sigma-Aldrich). Before measurements, cells were stained with a mix of anti-CD3–AF647 (clone UCTH1, Biolegend), anti-CD4–PE (clone RPA-T4, Biolegend) and anti-CD8–PECy5 (clone RPA-T8, Biolegend) antibodies. Dilution of fluorescent labels was measured in $CD3^+CD4^+$ T cells on FACSCalibur or FACSAria 4L SORP cell sorter flow cytometers (BD Biosciences). The percentage of proliferating $CD3^+CD4^+$ T cells was used as a read-out.

For unspecific stimulation of cytokine production, CFSE-labelled PBMC cultures after 7 days of incubation with specific antigens were added onto plates coated with anti-human CD3 monoclonal antibody (5 μg ml^{-1} in PBS, clone OKT3, Biolegend). After 12 h, brefeldin A (Sigma-Aldrich) was added to a concentration of 5 μg ml^{-1} for 3 h incubation at 37 °C, and then cells were stained with anti-CD3 and anti-CD4 antibodies (described above) for 30 min on ice. Intracellular staining was performed using a BD Cytofix/Cytoperm staining kit (BD Biosciences) according to the manufacturer's protocol. The following antibodies were used: anti-human IL-17A monoclonal antibody (clone BL168, labelled with AlexaFluor647, Biolegend, dilution 1:50), anti-human IFNγ monoclonal antibody (clone B27; labelled PacificBlue, dilution 1: 50) and isotype control antibodies (mouse IgG1k–PB and IgG1k–AF647, both from Biolegend).

ELISA for IFNγ and IL-17. PBMCs were cultured as described above the in presence of either human β-synuclein or MBP. After seven days in culture, supernatants were collected. An ELISA assay for detecting IFNγ and IL-17 concentrations was performed according to the manufacturer's protocol (R&D).

Statistical analysis. Statistical analysis was performed using GraphPad Prism 7.03 software (GraphPad Software). The tests performed and confidence intervals are indicated in the figure legends.

Reporting summary. Further information on research design is available in the Nature Research Reporting Summary linked to this article.

Data availability

The datasets generated during and/or analysed during the current study are available from the corresponding authors on reasonable request.

39. Lois, C., Hong, E. J., Pease, S., Brown, E. J. & Baltimore, D. Germline transmission and tissue-specific expression of transgenes delivered by lentiviral vectors. *Science* **295**, 868–872 (2002).
40. Määttä, J. A., Coffey, E. T., Hermonen, J. A., Salmi, A. A. & Hinkkanen, A. E. Detection of myelin basic protein isoforms by organic concentration. *Biochem. Biophys. Res. Commun*. **238**, 498–502 (1997).
41. Flügel, A., Willem, M., Berkowicz, T. & Wekerle, H. Gene transfer into $CD4^+$ T lymphocytes: green fluorescent protein-engineered, encephalitogenic T cells illuminate brain autoimmune responses. *Nat. Med*. **5**, 843–847 (1999).
42. Chmielewski, M. et al. T cells that target carcinoembryonic antigen eradicate orthotopic pancreatic carcinomas without inducing autoimmune colitis in mice. *Gastroenterology* **143**, 1095–107 (2012).
43. Doorn, K. J. et al. Brain region-specific gene expression profiles in freshly isolated rat microglia. *Front. Cell. Neurosci*. **9**, 84 (2015).
44. Torres-Nagel, N. E., Gold, D. P. & Hünig, T. Identification of rat Tcrb-V8.2, 8.5, and 10 gene products by monoclonal antibodies. *Immunogenetics* **37**, 305–308 (1993).
45. Smith, L. R., Kono, D. H. & Theofilopoulos, A. N. Complexity and sequence identification of 24 rat V beta genes. *J. Immunol*. **147**, 375–379 (1991).
46. Schläger, C., Litke, T., Flügel, A. & Odoardi, F. In vivo visualization of (auto) immune processes in the central nervous system of rodents. *Methods Mol. Biol*. **1304**, 117–129 (2014).
47. Schläger, C. et al. Effector T-cell trafficking between the leptomeninges and the cerebrospinal fluid. *Nature* **530**, 349–353 (2016).
48. Shevtsova, Z., Malik, J. M., Michel, U., Bähr, M. & Kügler, S. Promoters and serotypes: targeting of adeno-associated virus vectors for gene transfer in the rat central nervous system in vitro and in vivo. *Exp. Physiol*. **90**, 53–59 (2005).
49. Watanabe, T. et al. In vivo 3D MRI staining of the mouse hippocampal system using intracerebral injection of $MnCl_2$. *Neuroimage* **22**, 860–867 (2004).
50. Rauskolb, S. et al. Global deprivation of brain-derived neurotrophic factor in the CNS reveals an area-specific requirement for dendritic growth. *J. Neurosci*. **30**, 1739–1749 (2010).
51. Erny, D. et al. Host microbiota constantly control maturation and function of microglia in the CNS. *Nat. Neurosci*. **18**, 965–977 (2015).

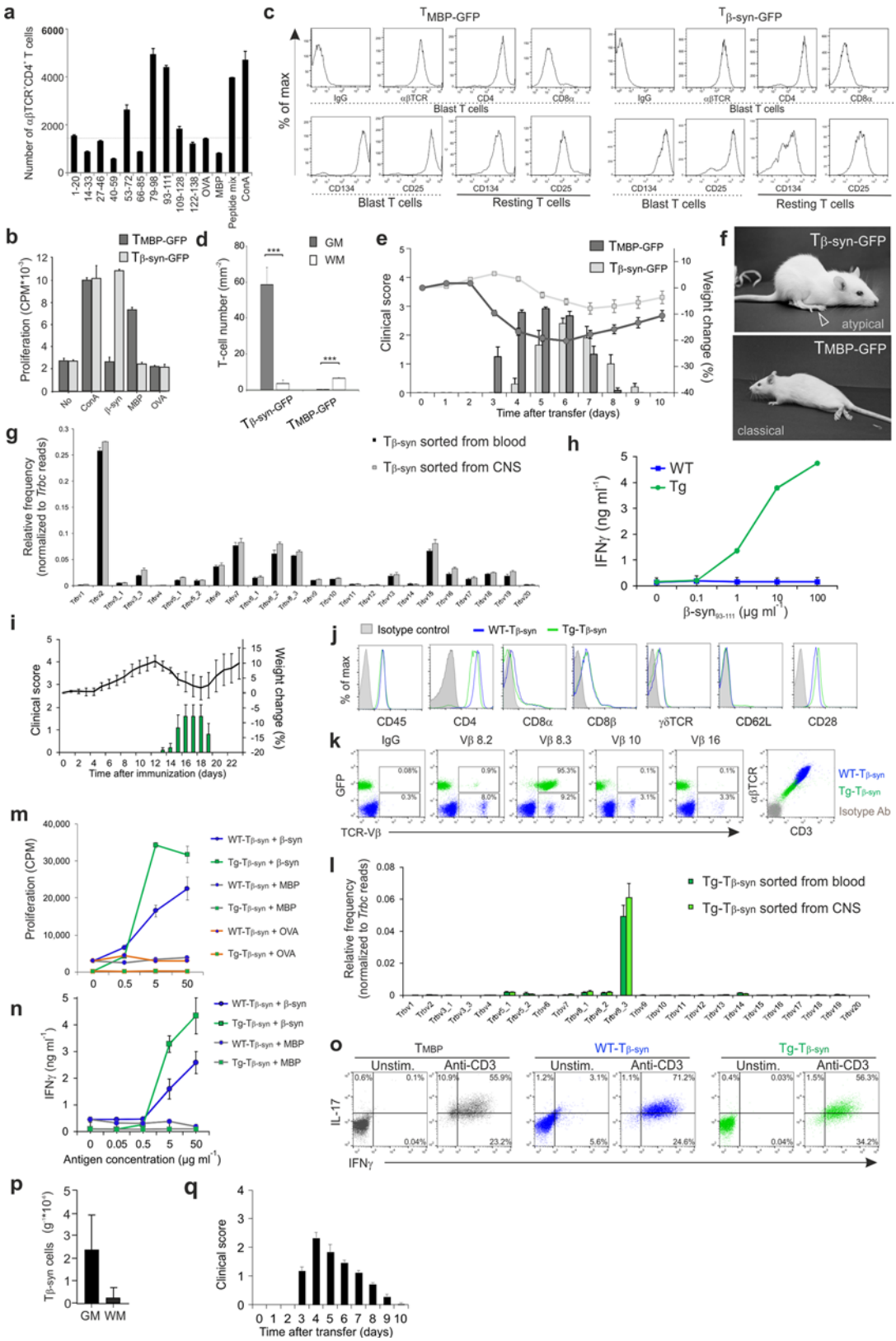

Extended Data Fig. 1 | See next page for caption.

Extended Data Fig. 1 | Characterization of wild-type and TCR-transgenic $T_{\beta\text{-syn}}$ cells in vitro and in vivo. a, Identification of the immunogenic β-synuclein peptides in Lewis rats. Screening of a β-synuclein peptide library covering the full-length protein for identification of immunogenic peptides. OVA, MBP, concanavalin A (ConA) and a mix of all peptides were used as control. The proliferation of $\alpha\beta TCR^+CD4^+$ T cells isolated from β-synuclein-immunized wild-type rats was measured by flow cytometry. Data are mean + s.e.m. from two independent experiments. **b**, Antigen response of established effector T cell lines. Wild-type $T_{\beta\text{-syn}}$ or T_{MBP} cell lines were cultured in the absence of antigen (No) or stimulated with ConA or the indicated antigens for 72 h. Proliferation was determined by ^{3}H-thymidine incorporation. Data are mean + s.e.m. Representative data of at least four independent experiments. **c**, Phenotype of $T_{\beta\text{-syn}}$ and T_{MBP} cell lines. Expression of αβTCR, CD4, CD8 and of surface activation markers CD134 and CD25 in cultured wild-type $T_{\beta\text{-syn}}$ and T_{MBP} cells. Flow cytometry was performed two days (blast T cells) and seven days (resting T cells) after antigen stimulation. IgG, isotype control. **d**, Histological quantification of $T_{\beta\text{-syn}}$ and T_{MBP} cells in cortical grey matter and corpus callosum (white matter) at the peak of T cell infiltration. Data are mean + s.e.m., $n = 5$ from 2 independent experiments. Unpaired two-tailed *t*-test. $^{***}P < 0.001$. **e**, Wild-type $T_{\beta\text{-syn}}$ cells induce clinical disease. Representative disease course upon intravenous transfer of wild-type $T_{\beta\text{-syn}}$ or T_{MBP} cells. Data are mean + s.d., $n = 6$–8 per group. Representative data of at least six independent experiments. **f**, Photographs illustrating frontlimb paralysis induced by $T_{\beta\text{-syn}}$ cells and classical EAE hindlimb paralysis induced by T_{MBP} cells. **g**, Expression of *Trbv* genes in wild-type $T_{\beta\text{-syn}}$ cells isolated ex vivo at the onset of $T_{\beta\text{-syn}}$ cell brain infiltration. Relative frequency was calculated in $T_{\beta\text{-syn}}$ cells from blood and CNS and expressed as ratio of reads mapping to a particular *Trbv* genomic segment to the number of reads mapping to the constant region of the TCR β chain encoded by *Trbc1* and *Trbc2* (RNA-seq analysis, $n = 3$ per group). Data are mean + s.d. **h**, Production of IFNγ by lymph node cells isolated from naive wild-type and TCR-transgenic (Tg) donors in response to $\beta\text{-syn}_{93–111}$ measured by ELISA. Data are mean ± s.d. **i**, Immunization of TCR-transgenic rats with $\beta\text{-syn}_{93–111}$ results in a monophasic clinical disease. Bars and lines indicate clinical score and relative weight change, respectively (mean ± s.d.). Representative data from two independent experiments ($n = 10$). **j**, Expression of surface markers on wild-type $T_{\beta\text{-syn}}$ (blue) and transgenic $T_{\beta\text{-syn}}$ (green) cell lines. **k**, TCR repertoire in transgenic $T_{\beta\text{-syn}}$ cell lines is dominated by transgenic TCR Vβ8.3 chain expression. **j**, **k**, Flow cytometry data. **l**, Expression of *Trbv* genes in transgenic $T_{\beta\text{-syn}}$ cell lines determined by RNA-seq analysis. Analysis and normalization of data as in **g**. $n = 3$ per group. **m**, **n**, Proliferative response measured by ^{3}H-thymidine incorporation (**m**) and IFNγ secretion measured by ELISA (**n**) in wild-type $T_{\beta\text{-syn}}$ (blue) and transgenic $T_{\beta\text{-syn}}$ (green) cell lines stimulated with the indicated amount of cognate (β-syn) or non-cognate (MBP, OVA) antigens. Data are mean ± s.d. **o**, Intracellular staining for IFNγ and IL-17 in T_{MBP} and $T_{\beta\text{-syn}}$ cell lines stimulated with anti-CD3 monoclonal antibodies. Representative data from at least three independently established T cell lines. **p**, Quantification of transgenic $T_{\beta\text{-syn}}$ cells infiltrating the cortical grey matter or the corpus callosum (white matter) measured by flow cytometry at the peak of T cell infiltration ($n = 5$). **q**, Clinical disease induced by transgenic $T_{\beta\text{-syn}}$ effector cells ($n = 15$). **p**, **q**, Data are mean + s.e.m.

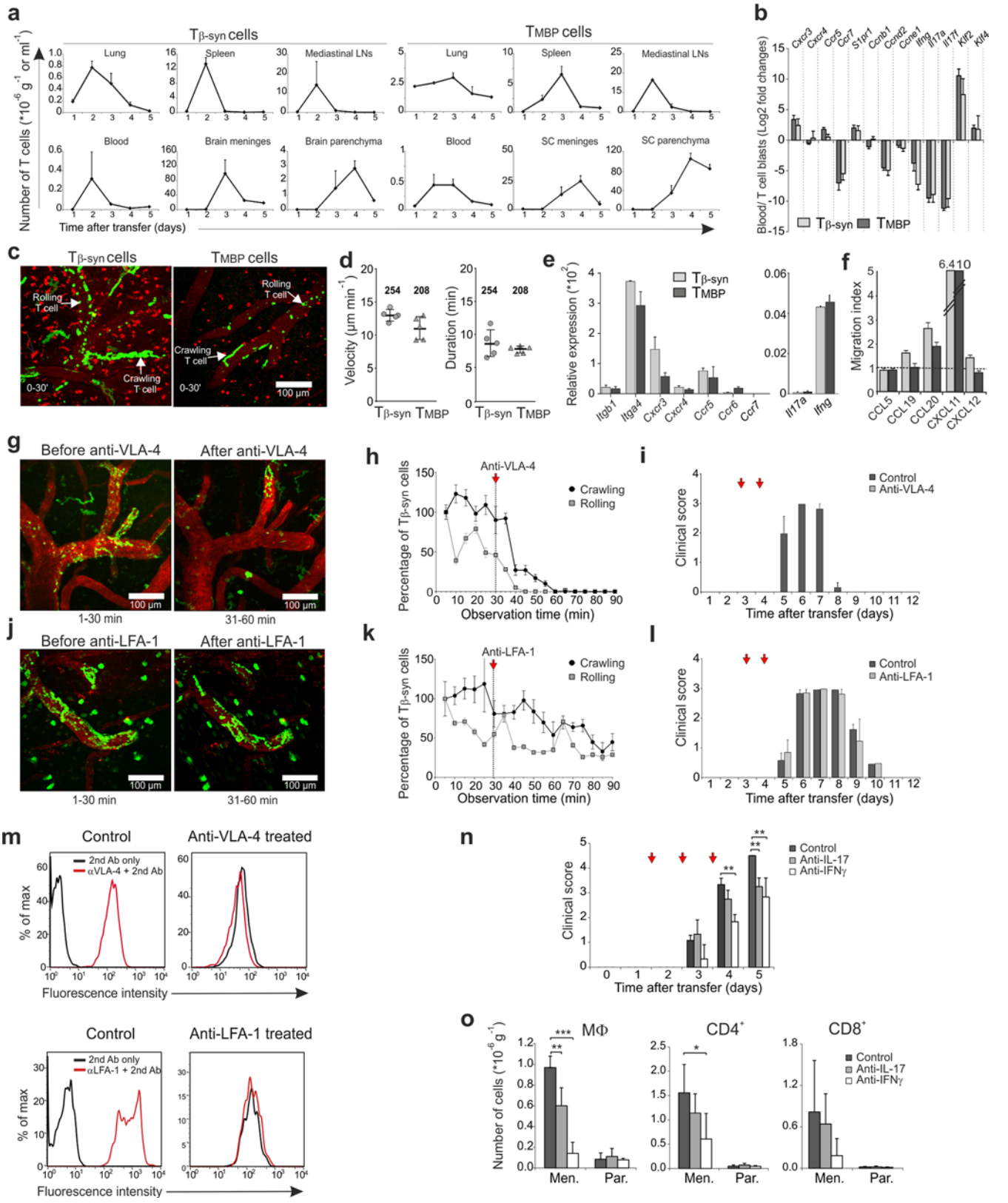

Extended Data Fig. 2 | See next page for caption.

Extended Data Fig. 2 | Migration properties and differentiation phenotype of $T_{\beta\text{-syn}}$ cells. a, $T_{\beta\text{-syn}}$ and T_{MBP} cells follow similar migratory routes before invading the CNS. Numbers of $T_{\beta\text{-syn}}$ and T_{MBP} cells in the indicated organs quantified every 24 h p.t. by flow cytometry. Data are mean + s.e.m. Representative data of three independent experiments including at least three rats per group per time point. **b**, $T_{\beta\text{-syn}}$ and T_{MBP} cells switch from an activated state to a migratory mode. Gene expression changes between migratory T cells (isolated from blood at the onset of CNS infiltration, that is, at day 3 p.t.) and in vitro T cells (24 h after antigen challenge) as measured by RNA-seq analysis. The ratio between the expression in migratory and in vitro activated T cells for the indicated genes is displayed. Data are mean + s.e.m., $n = 9$–15 per group from 3 independent experiments. **c**, **d**, $T_{\beta\text{-syn}}$ and T_{MBP} cells display very similar intravascular migration behaviour. Intravital TPLSM recordings were performed upon first arrival of $T_{\beta\text{-syn}}$ or T_{MBP} cells in the leptomeningeal brain vessels. **c**, Representative migratory path of $T_{\beta\text{-syn}}$ or T_{MBP} cells over a 30-min recording time. Rolling cells appear as multiple dots. Green, T cell tracks projected over time; red, blood vessels and leptomeningeal phagocytes. Representative data of at least four independent experiments (obtained from individual rats). **d**, Crawling velocity and track duration of $T_{\beta\text{-syn}}$ and T_{MBP} cells. Data are mean ± s.e.m. The number of analysed T cells is indicated. **e**, **f**, $T_{\beta\text{-syn}}$ and T_{MBP} cells are similar in integrin and cytokine expression and chemokine responsiveness. **e**, Relative expression (normalized to *Actb*) of the indicated integrins, chemokine receptors and cytokines as measured by quantitative PCR in $T_{\beta\text{-syn}}$ and T_{MBP} cells isolated from the blood at the onset of T cell CNS infiltration. Data are mean + s.d., $n = 3$ rats per group. **f**, Chemotactic response to the indicated chemokines of ex vivo-isolated $T_{\beta\text{-syn}}$ and T_{MBP} cells. Data are mean + s.d., $n = 2$ per group. **g**–**i**, VLA-4 crucially determines $T_{\beta\text{-syn}}$ cell invasion into the brain. **g**, **h**, $T_{\beta\text{-syn}}$ cell motility was recorded by intravital TPLSM upon first arrival of $T_{\beta\text{-syn}}$ cells in the leptomeningeal brain vessels before and immediately after intravenous injection of blocking anti-VLA-4 monoclonal antibody. **g**, Representative 30-min time-lapse recordings of $T_{\beta\text{-syn}}$ cell migratory paths. Green, 30-min $T_{\beta\text{-syn}}$ cell track projections; red, Texas red dextran-labelled vessels. Representative data of at least four independent experiments (obtained from individual rats). **h**, Percentage of crawling or rolling $T_{\beta\text{-syn}}$ cells before and after anti-VLA-4 monoclonal antibody treatment (arrow) relative to time point 0. Data are mean ± s.e.m. of $n = 3$. **i**, Clinical disease after applications of anti-VLA-4 or isotype monoclonal antibodies (control). Arrows indicate the time point of treatment. Data are mean + s.e.m. of $n = 4$ per group. Representative data of three independent experiments. **j**–**l**, LFA-1 integrin does not contribute to $T_{\beta\text{-syn}}$ cell invasion in the brain. Intravital TPLSM recordings were performed as in **g** before and after anti-LFA-1 monoclonal antibody administration. **j**, Representative 30-min time-lapse recordings of $T_{\beta\text{-syn}}$ cell migratory paths. Green, $T_{\beta\text{-syn}}$ cell tracks projected over time; red, Texas red dextran-labelled vessels. Representative data of at least four independent experiments (obtained from individual rats). **k**, Percentage of crawling or rolling $T_{\beta\text{-syn}}$ cells before and after monoclonal antibody treatment quantified as in **h**. Data are mean ± s.e.m. of $n = 3$. **l**, Disease course in $T_{\beta\text{-syn}}$ cell recipient rats treated either with anti-LFA-1 or isotype monoclonal antibodies (control) at the indicated time points (arrows). Data are mean + s.e.m. of $n = 4$ per group. Representative data of three independent experiments. **m**, Saturation of monoclonal antibody binding (in **g**–**i** and **j**–**l** experiments) was controlled by staining of blood-derived $T_{\beta\text{-syn}}$ cells with anti-VLA-4 or anti-LFA-1 primary monoclonal antibodies followed by secondary detection antibody (red) or with secondary antibody only (black). **n**, **o**, IL-17 or IFNγ blockade partially interferes with $T_{\beta\text{-syn}}$ cell entry into the brain. **n**, Disease course in $T_{\beta\text{-syn}}$-cell-transferred rats intrathecally treated at the indicate time points (arrows) with PBS (control), anti-IL-17 or anti-IFNγ monoclonal antibodies. Data are mean + s.e.m. of $n = 4$ per group. Representative data of three independent experiments. **o**, Quantification of macrophages (MΦ, $CD11b^+CD45^{high}$), $CD4^+$ and $CD8^+$ T cells infiltrating the brain leptomeninges and the brain parenchyma at the peak of clinical disease. Data are mean + s.e.m. of four rats per group. Representative data of two independent experiments. **n**, **o**, Unpaired two-tailed *t*-test. $^*P < 0.05$, $^{**}P < 0.01$, $^{***}P < 0.001$.

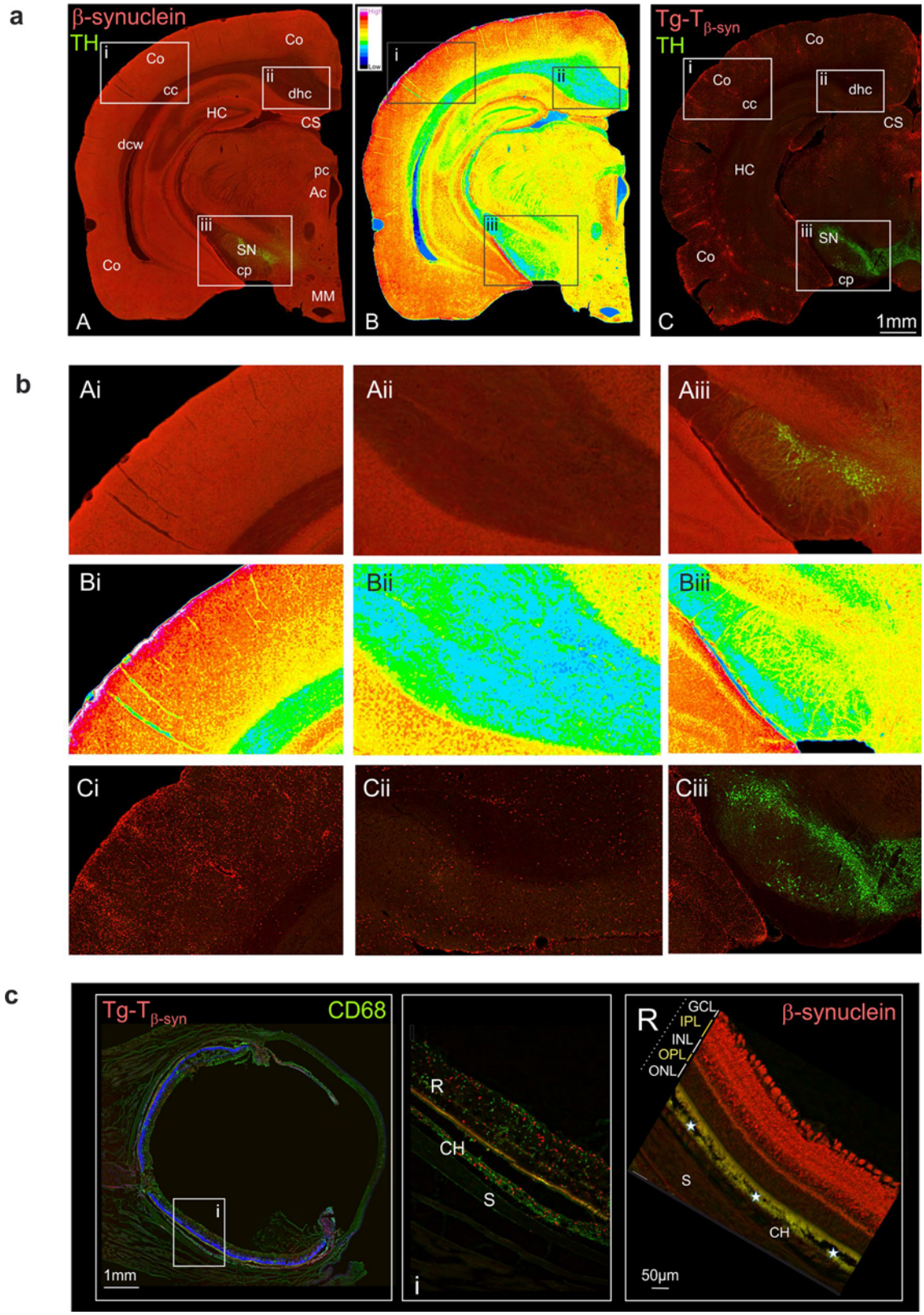

Extended Data Fig. 3 | $T_{β\text{-}syn}$ cell infiltration into CNS tissue correlates with β-synuclein expression. a, Coronal section of naive rat brain. Left, immunostaining for β-synuclein (red) and tyrosine hydroxylase (TH, green). Middle, colour-coded intensity of β-synuclein expression. Right, inflamed brain at the peak of $T_{β\text{-}syn}$ cell (red) infiltration. Green, TH. Co, cortex; HC, hippocampus; cc, corpus callosum; SN, substantia nigra; CS, colliculus superior; dhc, dorsal hippocampal commissure; cp, cerebral peduncle; dcw, deep cerebral white matter; Ac, aqueduct; MM, mammillary nucleus; pc, posterior commissure. **b**, Enlarged view of selected regions (i–iii) indicated by frames in **a**. **c**, Inflammatory infiltration of the eye. Left, cross-section at the peak of $T_{β\text{-}syn}$ cell (red) infiltration. Green, $CD68^+$ cells (activated microglia and macrophages). Enlarged view of a selected area (i) is shown in the middle panel. Right, β-synuclein expression within the eye (naive rat). Asterisks indicate the autofluorescent inner and outer segments of the photoreceptor cells. R, retina; CH, choroid; GCL, ganglion cell layer; IPL, inner plexiform layer; OPL, outer plexiform layer; INL, inner nuclear layer; ONL, outer nuclear layer; S, sclera.

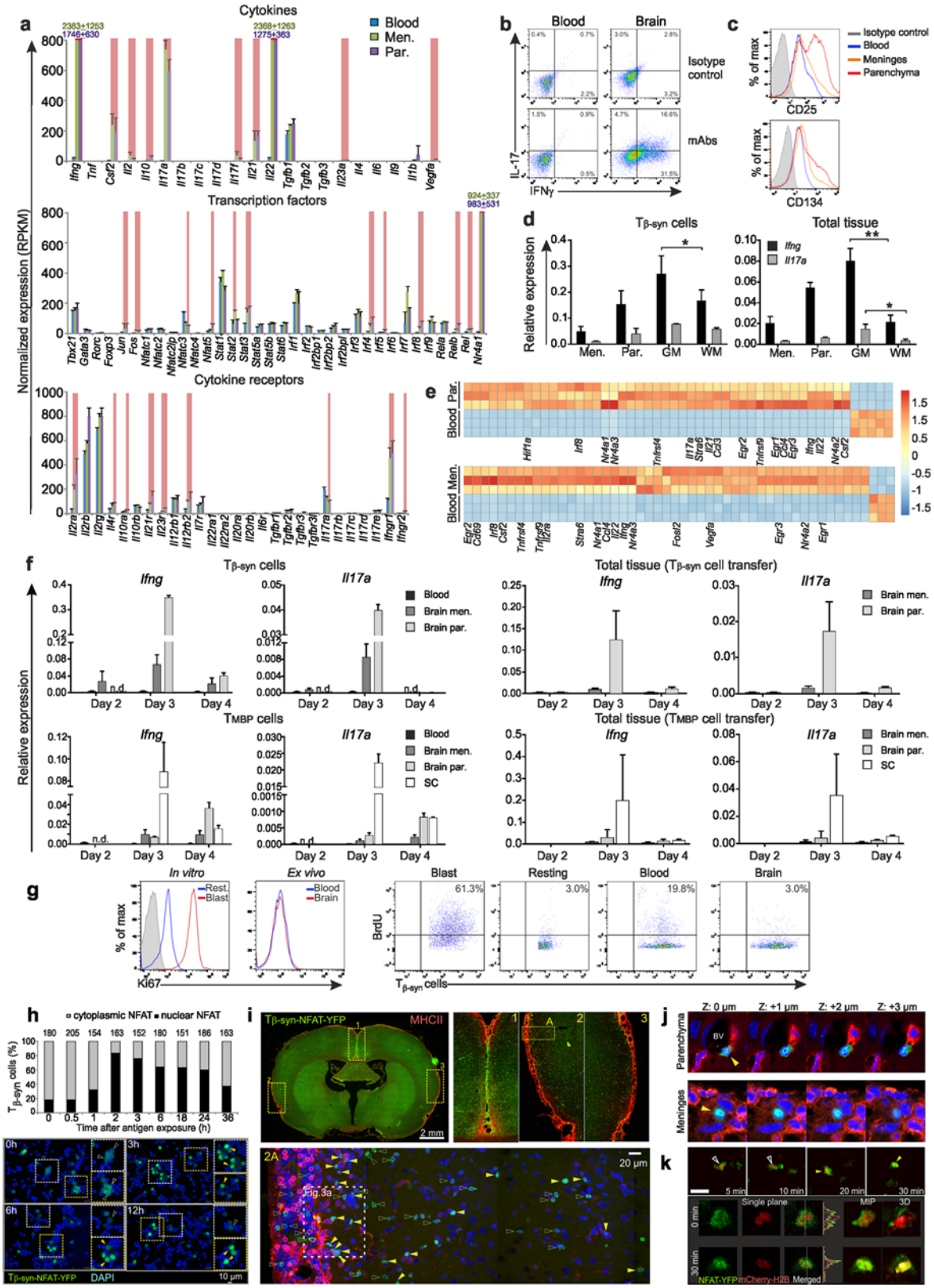

Extended Data Fig. 4 | See next page for caption.

Extended Data Fig. 4 | $T_{\beta\text{-syn}}$ cells are reactivated in the brain. **a**–**e**, $T_{\beta\text{-syn}}$ cells isolated from their target organ display an activated phenotype. **a**, Expression of selected sets of genes (grouped in functional classes) determined by RNA-seq analysis of $T_{\beta\text{-syn}}$ cells isolated from blood, brain meninges and brain parenchyma at the onset of $T_{\beta\text{-syn}}$ cell CNS infiltration. RPKM, reads per kilobase per million mapped reads. Data are mean + s.e.m., $n = 9$–15 per group from 3 independent experiments. Genes for which the expression in $T_{\beta\text{-syn}}$ cells from brain was significantly different from the expression in $T_{\beta\text{-syn}}$ cells from blood are highlighted by a red overlay colour. Unpaired two-tailed *t*-test. **b**, IFNγ and IL-17 expression (intracellular staining) in $T_{\beta\text{-syn}}$ cells isolated from blood and brain at the peak of T cell infiltration. Representative data of three independent experiments. **c**, Surface membrane activation marker (CD25 and CD134) expression in $T_{\beta\text{-syn}}$ cells isolated from the indicated compartments at the onset of $T_{\beta\text{-syn}}$ cell CNS infiltration determined by flow cytometry. **d**, Expression of *Ifng* and *Il17a* mRNA in $T_{\beta\text{-syn}}$ cells isolated from brain meninges, brain parenchyma, cortical grey matter and corpus callosum (white matter) measured by quantitative PCR (normalized to *Actb*). Data are mean + s.e.m. Representative data from two independent experiments. Unpaired two-tailed *t*-test. $^{*}P < 0.05$, $^{**}P < 0.01$. **e**, Top 50 differentially expressed genes in $T_{\beta\text{-syn}}$ cells isolated from blood, brain meninges and parenchyma at day 3 p.t. determined by RNA-seq. Heat map shows *z*-transformed relative expression values. Each column represents a gene, each row represents a biological replicate. Genes known to be regulated by TCR-driven activation are indicated. **f**, $T_{\beta\text{-syn}}$ cells, in contrast to T_{MBP} cells, are strongly activated in the brain. Left, *Ifng* and *Il17a* relative expression (normalized to *Actb*) in $T_{\beta\text{-syn}}$ or T_{MBP} cells isolated from blood or from the indicated CNS compartments at the indicated time points p.t. determined by quantitative PCR. Right, expression of the cytokines in the corresponding total CNS tissues. Data are mean + s.d. of three independent experiments. **g**, $T_{\beta\text{-syn}}$ cells do not proliferate in the brain. Histogram plots, Ki-67 expression of in vitro-cultured $T_{\beta\text{-syn}}$ cells (two and six days after antigenic stimulation) or of $T_{\beta\text{-syn}}$ cells isolated ex vivo from blood and brain at the peak of T cell infiltration. Grey, isotype control. Dot plots, corresponding quantification of BrdU incorporation. Representative data of three independent experiments. **h**, Kinetics of NFAT translocations in activated $T_{\beta\text{-syn–NFAT}}$ cells in vitro. Plot, quantification of T cells with nuclear or cytoplasmic NFAT reporter over the period of 36 h after stimulation. Numbers of counted $T_{\beta\text{-syn–NFAT}}$ cells are indicated. Representative fluorescent images showing $T_{\beta\text{-syn–NFAT}}$ cells with nuclear (closed arrowheads) or cytoplasmic (open arrowheads) NFAT reporter are shown. **i**–**k**, Detection of NFAT translocations in situ. **i**, Histologic analysis of brain tissue at the onset of disease. Top, fluorescent overview images of a coronal brain section with magnified views. bottom, selected region acquired at higher magnification. Green, $T_{\beta\text{-syn–NFAT}}$ cells; red, MHC class II^{+} cells; blue, DAPI (not depicted in the top panel). Filled and open arrowheads indicate T cells with nuclear and cytoplasmic localization of the NFAT–YFP reporter, respectively. Dashed line indicates the position of an area presented in Fig. 3a. **j**, Confocal images showing representative $T_{\beta\text{-syn–NFAT}}$ cells with nuclear NFAT reporter in the parenchyma and meninges of the cortex. Individual *z* planes. **k**, In vivo visualization of de novo NFAT reporter translocation. Top, intravital TPLSM recording of NFAT translocation from the cytoplasm (open arrowhead) to the nucleus (closed arrowhead). Bottom, single *z* planes (shown as single colours and merged channels), maximum intensity projections (MIP) and 3D-rendered images depict the same $T_{\beta\text{-syn–NFAT-CherryH2B}}$ cell before (0 min) and after (30 min) NFAT translocation. Histogram profile shows YFP and mCherry fluorescence intensities along the line indicated on the adjacent image.

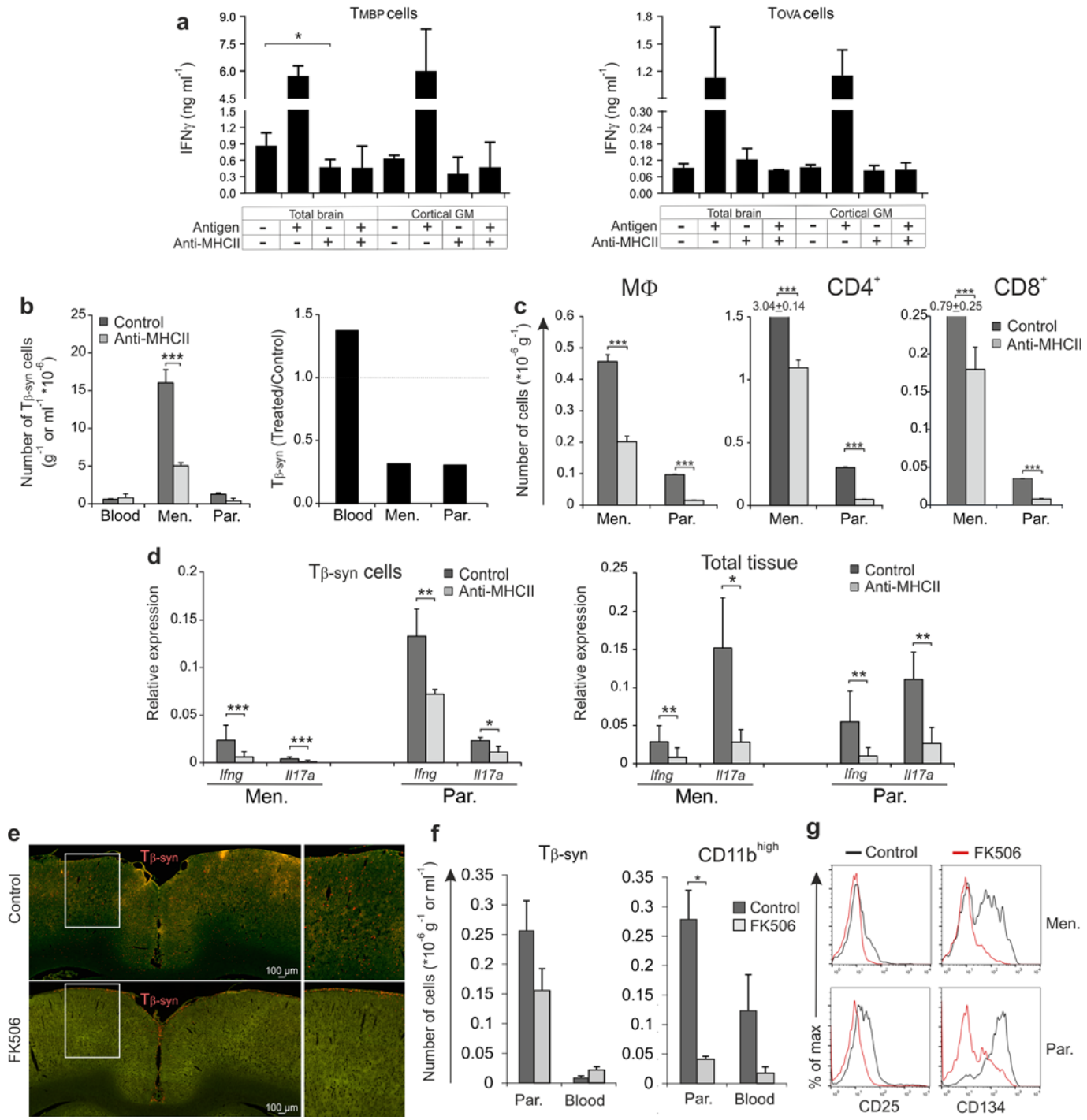

Extended Data Fig. 5 | Activation of $T_{\beta\text{-syn}}$ cells within the brain is critical for their infiltration and for secondary immune cell recruitment and clinical disease. a, Microglia from CNS grey matter is inefficient to present antigen to T_{MBP} cells. Microglial cells isolated from brain parenchyma (total brain) or from cortical grey matter were cocultured for 48 h with T_{MBP} cells (left) or T_{OVA} cells (right) with or without addition of cognate antigen. Anti-MHC class II blocking monoclonal antibodies or PBS were added for each condition. IFNγ production was measured by ELISA. Representative data from three independent experiments per cell type. Data are mean + s.e.m., $n = 3$. **b**–**d**, Blocking antigen presentation in vivo by intrathecal injection of anti-MHC class II monoclonal antibody prevents $T_{\beta\text{-syn}}$ cell entry into the brain and local reactivation. **b**, Number of $T_{\beta\text{-syn}}$ cells in blood, brain meninges and brain parenchyma in rats treated with PBS (control) or anti-MHC-II monoclonal antibodies quantified at the onset of disease and the corresponding rate of infiltration in the brain compartments normalized to blood. Flow cytometry data. **c**, Quantification of the number of macrophages ($CD11b^{+}CD45^{high}$ cells), $CD4^{+}$ and $CD8^{+}$ T cells recruited to the indicated brain compartments. **b**, **c**, Representative data of two independent experiments including at least three rats per group. **d**, Relative expression of inflammatory cytokines (normalized to *Actb*) either in $T_{\beta\text{-syn}}$ cells isolated from the indicated brain compartments (left) or in brain tissues (right) assessed by quantitative PCR. Data are mean + s.e.m. of $n = 3$. Representative data of two independent experiments. **e**–**g**, Effect of FK506 treatment on the infiltration of $T_{\beta\text{-syn}}$ cells into the grey matter of the brain. **e**, Coronal brain sections (fluorescence overview images and magnified views of selected areas) from control (clinical score 1.5) or FK506-treated (clinical score 0) rats. Red, $T_{\beta\text{-syn}}$ cells; green/yellow, tissue autofluorescence. **f**, Numbers of $T_{\beta\text{-syn}}$ cells and recruited myeloid cells ($CD11b^{high}$) in the indicated compartments determined by flow cytometry. Data are mean + s.e.m., $n = 3$ per group. **g**, Expression of CD25 and CD134 on $T_{\beta\text{-syn}}$ cells. **a**, One-way ANOVA with Dunnet's correction for multiple comparison. **b**–**d**, **f**, Unpaired two-tailed *t*-test. $^{*}P < 0.05$, $^{**}P < 0.01$, $^{***}P < 0.001$.

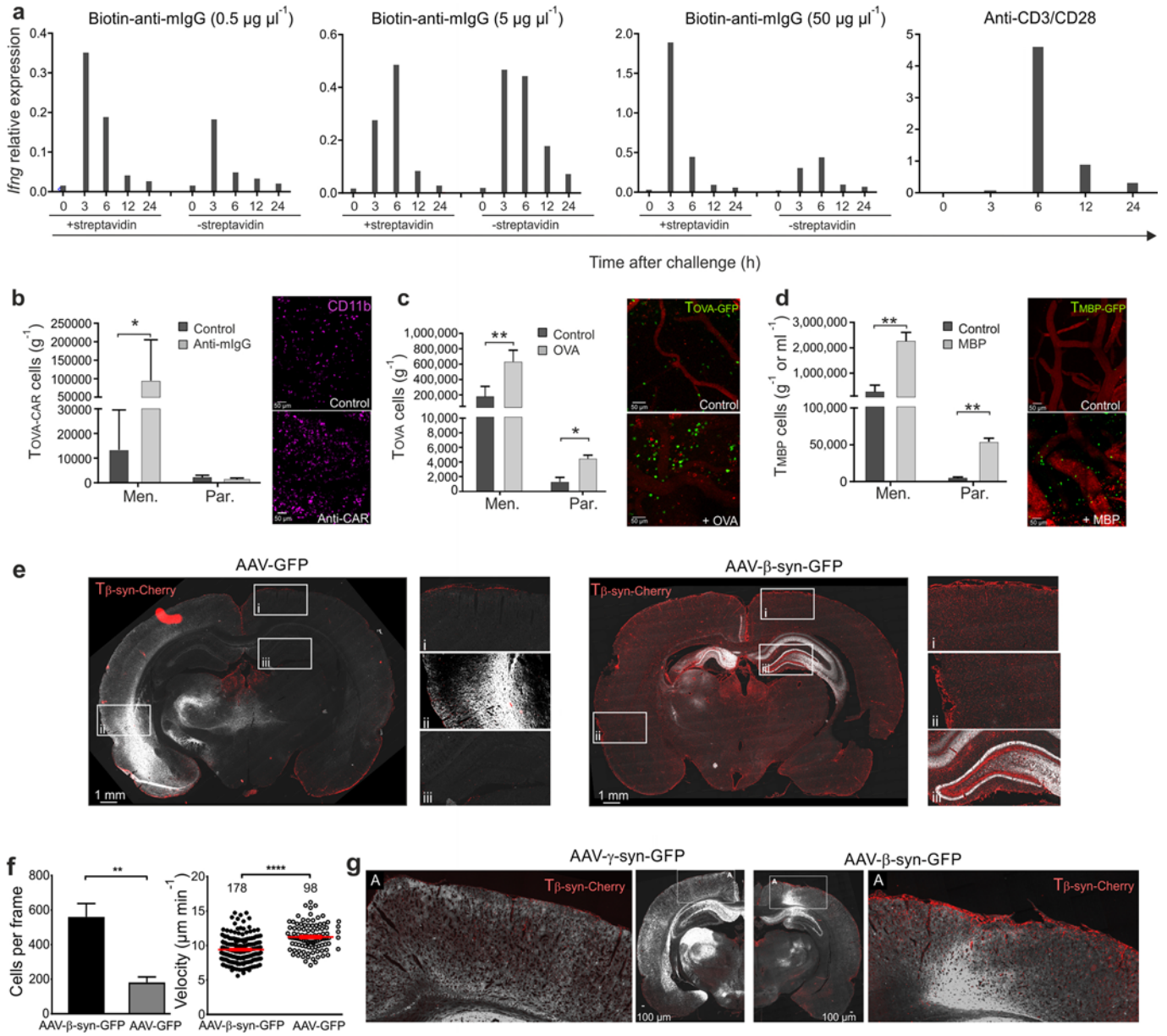

Extended Data Fig. 6 | Antigen availability determines T cell infiltration into the brain. a, In vitro activation of $T_{OVA-CAR}$ cells. Relative expression of IFNγ in $T_{OVA-CAR}$ cells challenged in vitro with biotin anti-mouse IgG at the indicated doses in the presence or absence of streptavidin. Quantitative PCR performed at the indicated time points after challenge. Stimulation of $T_{OVA-CAR}$ cells at the matching time points with anti-CD3/CD28 is shown as comparison (right plot) (normalized to β-actin). **b**, In vivo activation prompts $T_{OVA-CAR}$ and myeloid-cell entry into the brain. Plot, number of $T_{OVA-CAR}$ cells in brain meninges and brain parenchyma quantified by flow cytometry 3 days p.t. Rats were injected intrathecally or i.c.v. with biotin anti-mouse IgG (anti-CAR) 6 h before analysis, to trigger T cell activation. Control, PBS-treated animals. Data are mean + s.e.m. Cumulative data of three independent experiments including two animals per group. Intravital TPLSM images of the brain cortex three days p.t. are shown. $T_{OVA-CAR}$ cells show infiltration of $CD11b^+$ cells labelled by intrathecal injection of SeTau647-conjugated anti-CD11b monoclonal antibodies (magenta). Recordings were performed 6 h after i.c.v. injection of PBS (control) or anti-mouse IgG1 (anti-CAR). **c**, **d**, Effector T cell entry into the brain is boosted by increased antigen availability. Plots, quantification of T_{OVA} cells (**c**) or T_{MBP} cells (**d**) in the indicated brain compartments 3 days p.t. Rats were injected i.c.v. with the cognate antigen 12 h before analysis. $n = 2$ per T cell specificity. Corresponding intravital TPLSM images are shown. Green, antigen-specific T cells; red, blood vessels and macrophages. **e**–**g**, Neuronal overexpression of β-synuclein strongly increases $T_{β\text{-}syn}$ cell invasion into the brain. **e**, Fluorescence overview images and magnified views of selected areas of coronal brain sections depicting the pattern of $T_{β\text{-}syn}$ cell infiltration at the peak of the T cell grey matter infiltration. The rats had been neonatally injected with AAVs expressing GFP or β-syn–GFP under the synapsin promoter. Representative data of three independent experiments. Red, $T_{β\text{-}syn}$ cells; Grey (false colour), GFP- or β-synuclein-expressing neurons. **f**, Quantitative analyses of $T_{β\text{-}syn}$ cells by intravital TPLSM in AAV-β-syn-GFP or AAV-GFP rats. Number of grey-matter-infiltrating $T_{β\text{-}syn}$ cells (left) and their velocity over a 30-min period (right). Note the decreased speed of $T_{β\text{-}syn}$ cells in rats overexpressing β-synuclein, indicating local T cell activation. $n = 2$ from 2 independent experiments. **g**, Neuronal overexpression of β- but not γ-synuclein increases $T_{β\text{-}syn}$ cell entry into the brain. Fluorescence overview pictures and magnified cortical areas at the peak of $T_{β\text{-}syn}$ cell infiltration depicting the infiltration pattern of $T_{β\text{-}syn}$ cells into the brain of rats overexpressing β- or γ-synuclein in neurons. Red, $T_{β\text{-}syn}$ cells; grey (false colour), neurons overexpressing β- or γ-synuclein. Representative data of two independent experiments. **b**–**d**, Unpaired two-tailed *t*-test. **f**, Mann–Whitney *U*-test. $^*P < 0.05$, $^{**}P < 0.01$, $^{***}P < 0.001$, $^{****}P < 0.001$.

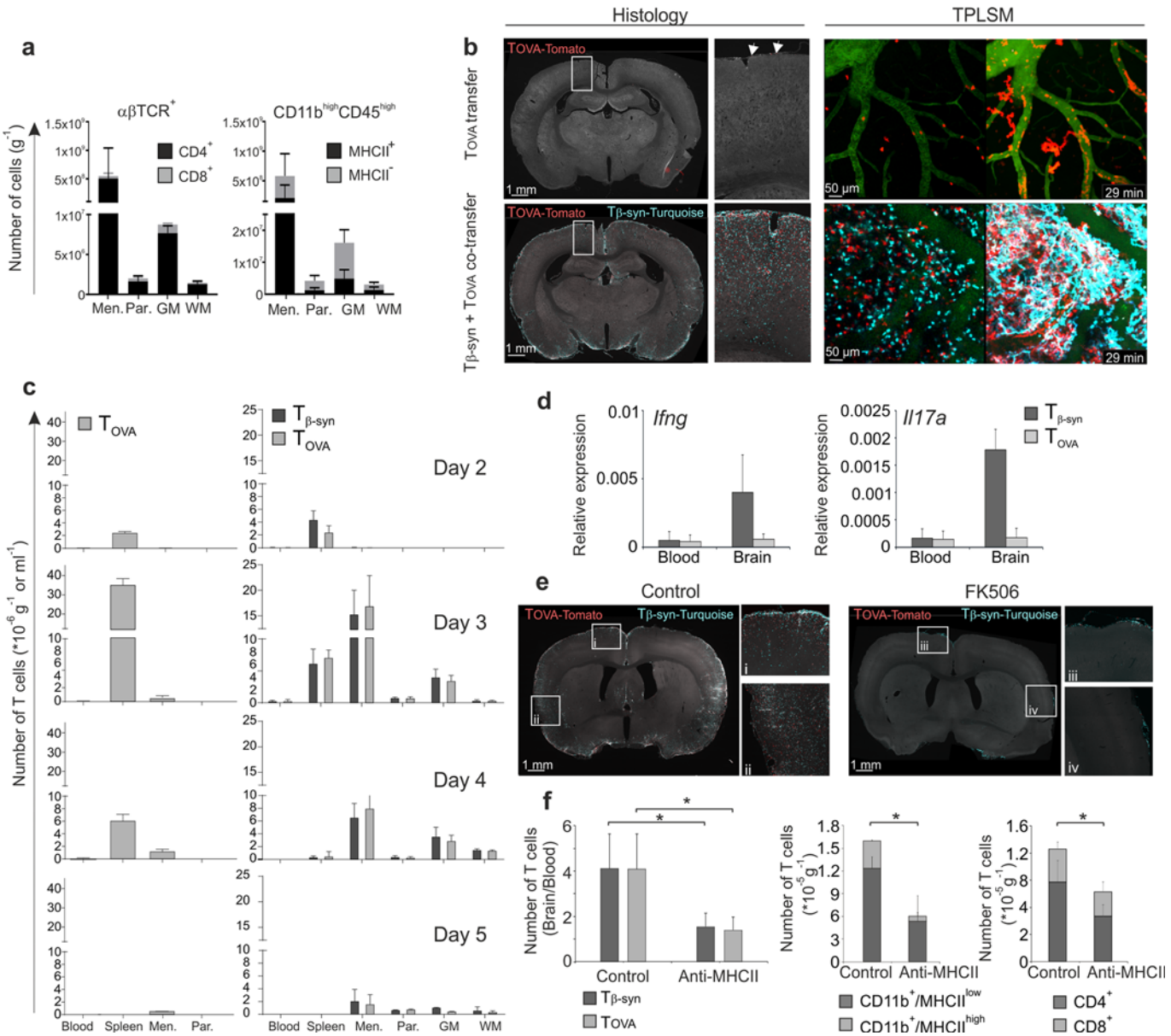

Extended Data Fig. 7 | $T_{\beta\text{-syn}}$ cell activation drives immune cell recruitment. a, Recruitment of host T cells and myeloid cells determined by flow cytometry at the peak of disease induced by $T_{\beta\text{-syn}}$ cell transfer. Data are mean + s.e.m., $n = 3$. **b–d**, $T_{\beta\text{-syn}}$ cell invasion in the CNS drives recruitment of CNS-ignorant T_{OVA} cells. **b**, T_{OVA} cell recruitment to the grey matter cortex after transfer of $T_{OVA\text{–}Tomato}$ cells alone (top) or after cotransfer with $T_{\beta\text{-syn–}Turquoise}$ cells (bottom). Left, fluorescence overview images and magnified views of selected areas of coronal brain sections. Right, TPLSM individual stacks and corresponding migratory paths of $T_{\beta\text{-syn}}$ and/or T_{OVA} cells over a 30-min recording time. Data were acquired 3.5 days after T cell transfer. Arrows point to representative T_{OVA} cells. Red, T_{OVA} cells; turquoise, $T_{\beta\text{-syn}}$ cells, green, blood vessels (labelled by FITC-conjugated dextran). Representative data of at least three independent experiments (obtained from individual rats). **c**, Time course of T cell infiltration in the indicated compartments upon single transfer of $T_{OVA\text{–}Tomato}$ cells or cotransfer of $T_{\beta\text{-syn–}Turquoise}$ and $T_{OVA\text{–}Tomato}$ cells, determined by flow cytometry. Data are mean + s.e.m., $n = 3$ per time point. Representative data of two independent experiments. **d**, T_{OVA} cells are not reactivated in the brain. Expression level of the indicated cytokines measured by quantitative PCR in $T_{\beta\text{-syn}}$ and T_{OVA} cells isolated from the indicated compartments upon cotransfer. Data are mean + s.e.m., $n = 3$. Representative data of two independent experiments. **e**, FK506 treatment prevents T_{OVA}-cell recruitment to the grey matter tissue. Fluorescence overview images as in **b** from control (clinical score 2) or FK506-treated (clinical score 0) rats 3.5 days after cotransfer. Representative images of two independent experiments including three rats per group. **f**, Blockade of antigen presentation by intrathecal administration of anti-MHCII monoclonal antibodies effectively reduces immune cell recruitment to the brain in the cotransfer experiment. Left, ratio of the numbers of $T_{\beta\text{-syn}}$ or T_{OVA} cells in brain tissue to the number of $T_{\beta\text{-syn}}$ or T_{OVA} cells in blood. Data are mean + s.e.m., $n = 3$. Middle and right, absolute number of myeloid cells or T cells in the brain tissue measured by flow cytometry 3.5 days after cotransfer of $T_{\beta\text{-syn}}$ and T_{OVA} cells. Data are mean + s.e.m., $n = 3$. **f**, Unpaired two-tailed *t*-test. $^*P < 0.05$.

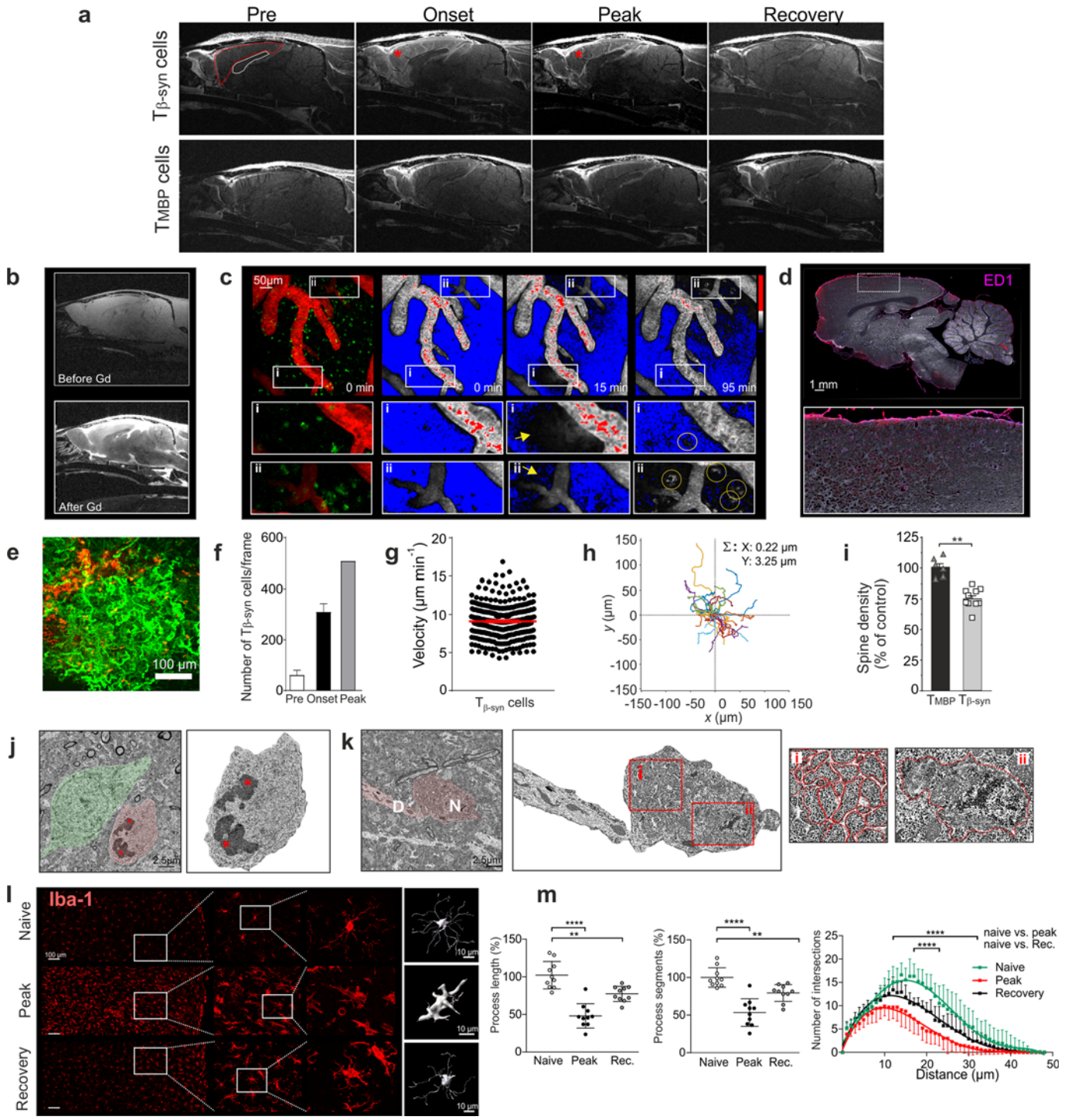

Extended Data Fig. 8 | See next page for caption.

Extended Data Fig. 8 | Inflammatory changes to the brain tissue during acute disease induced by transfer of $T_{\beta\text{-syn}}$ cells. a–d, $T_{\beta\text{-syn}}$ cell infiltration into the brain leptomeninges is associated with BBB leakage. **a**, Representative T1-weighted MRI images highlighting the areas of Gd leakage in meninges and parietal cortex over an EAE course induced by $T_{\beta\text{-syn}}$ or T_{MBP} cell transfer. **b–d**, MRI, intravital TPLSM and immunohistochemistry were performed in the same rat at the onset of $T_{\beta\text{-syn}}$-cell-induced disease. **b**, T1-weighted MRI images before and after Gd administration. **c**, TPLSM images. Left, infiltration pattern of $T_{\beta\text{-syn}}$ cells (green) into the leptomeninges. Red, Texas red dextran-labelled vessels, macrophages. Right, colour-coded (HiLo LUT) images highlighting the areas of dye leakage (arrows). Saturated signal, red; no signal, blue; circles, meningeal phagocytes that took up the dye during the recording time. Shown are tile-scan overview images (top) and magnified views of selected areas (bottom). **d**, Overview fluorescence image of a sagittal brain section (top) and magnified view of a selected cortical area (bottom) stained for ED1. Note the presence of high numbers of recruited $ED1^+$ myeloid cells (purple) in meninges and adjacent cortex. **e–h**, Migration behaviour of $T_{\beta\text{-syn}}$ cells in the cortical grey matter. Intravital TPLSM recording performed at the peak of $T_{\beta\text{-syn}}$ cell cortical infiltration reveals a vigorous migratory activity of the $T_{\beta\text{-syn}}$ cells within the compact grey matter. **e**, The 30-min time-lapse trajectories. **f**, Number of infiltrating $T_{\beta\text{-syn}}$ cells. Data are mean + s.e.m., $n = 3$. **g**, $T_{\beta\text{-syn}}$ cell velocity ($n = 340$ cells). **h**, Superimposed trajectories over a 30-min time span recording. Σ, sum of all cell trajectory vectors divided by the number of cells ($n = 30$ cells, each line represents a cell). **i–k**, $T_{\beta\text{-syn}}$ cell infiltration induces neuronal damage. Histological and electron microscope analyses at the peak of $T_{\beta\text{-syn}}$ cell infiltration. **i**, Relative changes in spine density on apical dendrites (cortical layer 2/3) measured by confocal microscopy in brain slices of rats transferred with the indicated antigen-specific T cells. Each dot represents a separate rat. Data are mean + s.e.m. **j**, Electron micrograph of an apoptotic neuron (highlighted in red, magnified view shown on the right) with a pyknotic and fragmented nucleus (asterisks) next to an intact neuron (green) with euchromatic nucleus. **k**, Apoptotic pyramidal neuron (N) with numerous apoptotic bodies (i) and pyknotic nucleus (ii) shown at higher magnification. Note the dendritic process (D) that emerges from the strongly altered cell body. **l, m**, $T_{\beta\text{-syn}}$ cell infiltration induces microglial activation. **l**, Anti-IBA1 staining of cortical tissue performed at the indicated time points after $T_{\beta\text{-syn}}$ cell transfer. Overviews pictures with magnified areas and representative 3D-reconstructed images of $IBA1^+$ microglial cells (shown in greyscale). **m**, Quantification of the morphological parameters of $IBA1^+$ microglial cells. Data are mean + s.d. **i**, Mann–Whitney *U*-test. **m**, One-way ANOVA with Dunnett's multiple comparison correction for process length and segments and two-way ANOVA with Sidak correction for multiple comparisons for number of intersections. $^{**}P < 0.01$, $^{***}P < 0.001$, $^{****}P < 0.0001$.

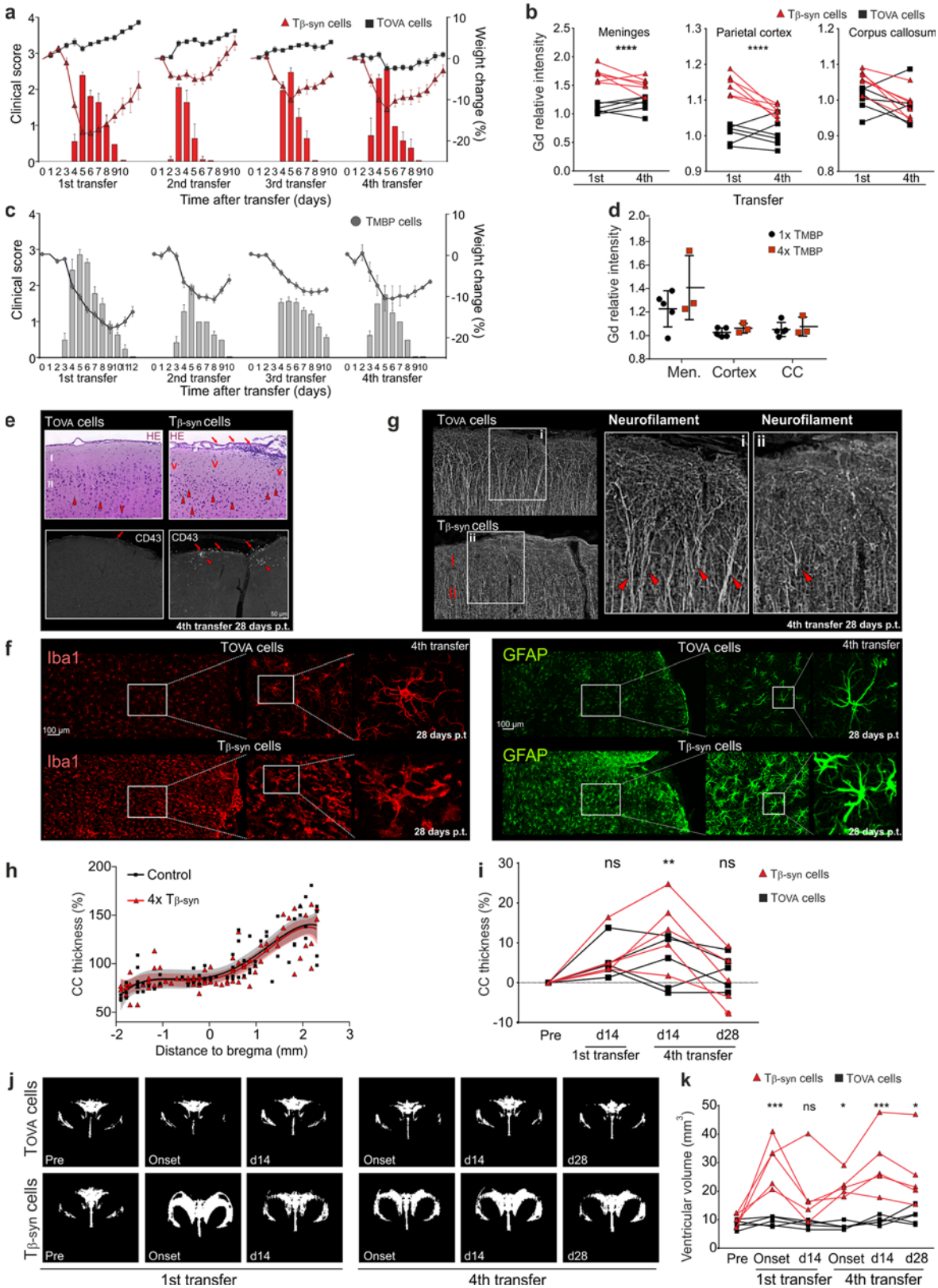

Extended Data Fig. 9 | See next page for caption.

Extended Data Fig. 9 | Consecutive $T_{\beta\text{-syn}}$ cell attacks result in cortical grey matter degeneration. a, Relapsing-remitting clinical disease bouts induced by repeated $T_{\beta\text{-syn}}$ cell transfer. Clinical score (bars) and relative weight changes (lines) in transgenic rats transferred four consecutive times with $T_{\beta\text{-syn}}$ or T_{OVA} cells. Data are mean ± s.e.m. Representative data of four independent experiments. **b**, Consecutive $T_{\beta\text{-syn}}$-cell-mediated grey matter inflammation induces reiterated episodes of BBB leakage. Quantification of Gd enhancement in the indicated brain compartments performed on T1-weighted MRI images acquired at the onset of disease after the first and fourth T cell transfer. Each line represents one individual rat. Representative data of 2 independent experiments ($n = 5$ per group per experiment). **c**, Relapsing-remitting clinical disease bouts induced by repeated T_{MBP} cell transfer. Clinical score (bars) and relative weight changes (lines) in transgenic rats transferred four consecutive times with T_{MBP} cells. Data are mean ± s.e.m. **d**, T_{MBP}-cell-induced disease bouts do not cause BBB leakage. Quantification of Gd enhancement in the indicated brain compartments performed as in **b**. **e**–**i**, Repeated $T_{\beta\text{-syn}}$-cell-induced autoimmune inflammation induces long-term damage in the cortical grey matter. Rats were transferred four times with $T_{\beta\text{-syn}}$ or T_{OVA} cells. Histological analysis of the cerebral cortex was performed three weeks after the peak of the fourth disease bout. **e**, Very few residual immune infiltrates are detectable in the recovery stage of relapsing grey matter disease. Top, representative haematoxylin and eosin (HE)-stained coronal paraffin sections of brain cortex showing the presence of very limited infiltrates in the leptomeninges (arrows) of a 4× $T_{\beta\text{-syn}}$ cell-transferred rat. Note, however, the thickened leptomeninges, increased vascularization (V) in the cortical layer I (I) and enrichment of cells with small nuclei, representing microglia (examples shown by arrowheads). Bottom, representative CD43 (W3/13) staining on frozen sections of 4× T_{OVA} and 4× $T_{\beta\text{-syn}}$ cell-transferred rats. The latter shows few $CD43^+$ lymphocytes within the leptomeninges (arrows) and around cortical vessels (arrowheads). **f**, Persistent grey matter gliosis induced by 4× $T_{\beta\text{-syn}}$ cell transfer. Confocal images of cortical tissue stained with anti-IBA1 (left) or anti-GFAP antibodies (right). **g**, Rarefaction and disarrangement of neuronal processes. Representative neurofilament stainings of cortical grey matter on 4× $T_{\beta\text{-syn}}$ or 4× T_{OVA}-cell-transferred rats. In corresponding regions of the motor cortex, the thickness, length and number of straight filaments (arrowheads) are reduced in rats that have received 4× $T_{\beta\text{-syn}}$ cells. **h**, **i**, Repeated episodes of grey matter inflammation do not affect white matter thickness. **h**, Histological analysis of corpus callosum thickness. Mean corpus callosum thickness across all control samples for the analysed anterior–posterior interval was set to 100%. Each data point represents relative corpus callosum thickness for one individual rat measured at the indicated distance to bregma. Lines represent fitting curves (shading, 95% confidence interval) for the respective group of rats. $n = 8$ for control, $n = 6$ for 4× $T_{\beta\text{-syn}}$ group from 4 independent experiments. Unpaired two-tailed t-test. **i**, Corpus callosum thickness determined by longitudinal MRI analysis at the indicated time over the disease course. Each line represents one individual rat. Representative data of 2 independent experiments ($n = 5$ per group per experiment). **j**, **k**, Enlargement of the ventricle size induced by relapsing autoimmune grey matter disease. **j**, Representative z projection of MRI images at the indicated time points after the first and fourth transfer of $T_{\beta\text{-syn}}$ or T_{OVA} cells. **k**, Quantification of changes in ventricular volume over time. Representative data of 2 independent experiments ($n = 5$ per group per experiment). **b**, **i**, **k**, Two-way ANOVA with Bonferroni's multiple comparison correction. $^*P < 0.05$, $^{**}P < 0.01$, $^{***}P < 0.001$, $^{****}P < 0.0001$.

a

	Control	RRMS	SPMS	PPMS	PD
Number	29	19	10	11	20
Age, years±SD	48.4±22.0	31.8±7.8	53.4±12.5	61.7±7.7	68.8±8.1
Females, number - (%)	17 (58.6)	11 (57.9)	6 (60)	3 (27.3)	9 (45)
Mean EDSS score±SD		1.79±0.99	6.15±1.75	4.60±1.29	
Mean Hoen and Yahe score±SD					2.83±0.83
Disease duration, years±SD		5.89±3.38	22.6±13.04	8.40±4.83	8.83±5.02
Diseease modyfing therapy, number - (%)					
Interferon		4 (21.1)			
Glatiramer acetate		4 (21.1)			
Fingolimod		2 (10.5)			
Dimethylfumarate		1 (5.3)			
GCC interval therapy			6 (60)	7 (63.6)	
Mitoxantrone			2 (20)		
None		3 (15.8)	2 (20)	1 (9.1)	

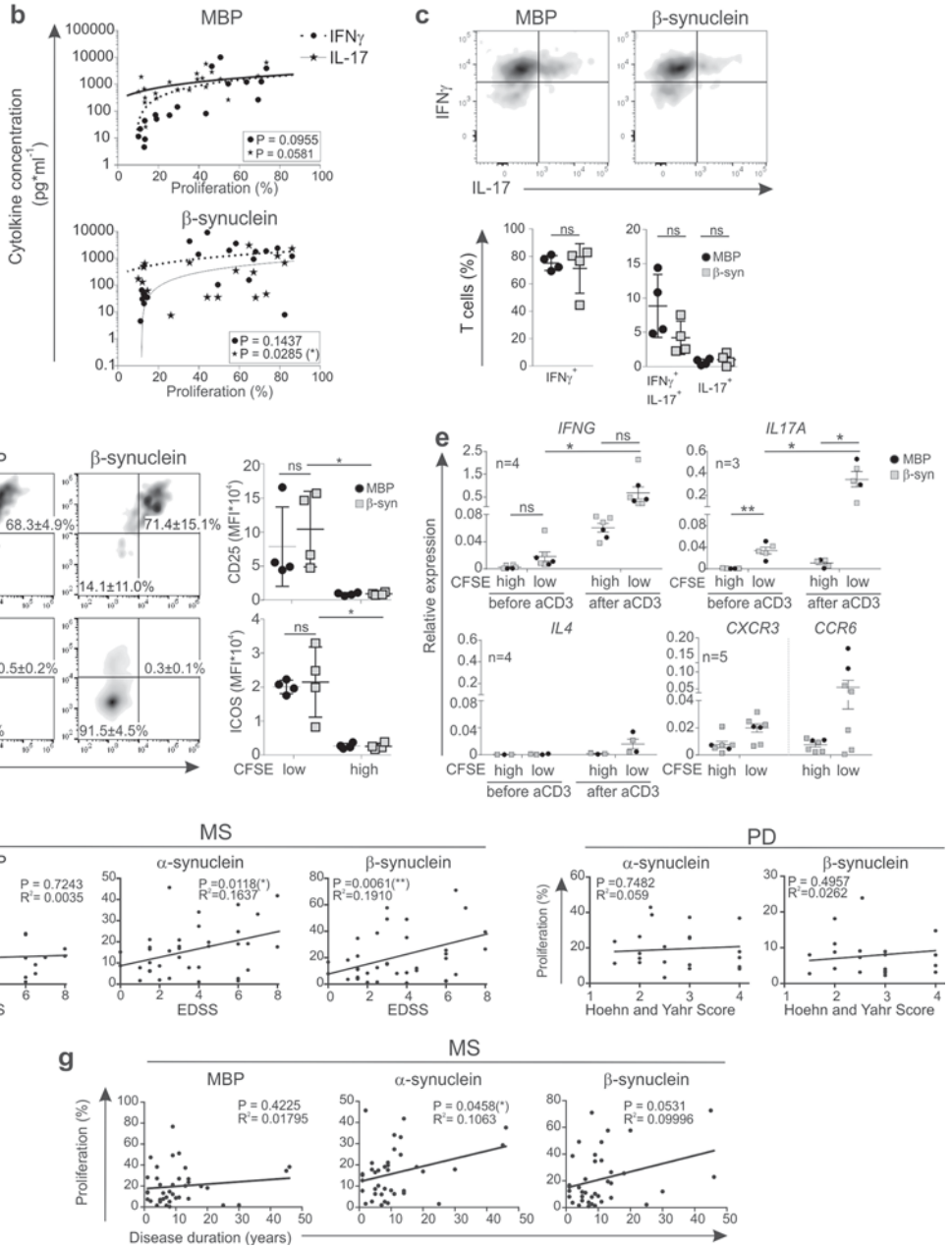

Extended Data Fig. 10 | See next page for caption.

Extended Data Fig. 10 | Cytokine and chemokine receptor expression of myelin-reactive and neuronal-antigen-reactive T cells. a, Characteristics of the donor cohort. **b**, Correlation between cytokine production (ELISA) and $CD4^+$ T cell proliferation. PBMCs were stimulated with the indicated antigens. Each dot represents one patient. **c**, IFNγ and IL-17 production in the proliferating $CD4^+$ T cells ($n = 3$). **d**, CD25 and ICOS expression in proliferating ($CFSE^{low}$) and non-proliferating ($CFSE^{high}$) $CD4^+$ T cells. Flow cytometry seven days after antigenic stimulation. Representative density plots (numbers indicate frequencies as mean + s.d. percentages, $n = 3$) and quantification of mean fluorescence intensities (MFI, $n = 4$). **e**, Gene expression levels of *IFNG*, *IL17A*, *IL4*, *CXCR3* and *CCR6*, determined by quantitative PCR (normalized to *RPL13A*). PBMCs isolated from patients with MS were stimulated with MBP or β-synuclein. After seven days, cytokine expression was determined in proliferating ($CFSE^{low}$) and non-proliferating ($CFSE^{high}$) $CD3^+CD4^+$ T cells before and after stimulation with CD3 antibodies. Chemokine expression was determined just before CD3 stimulation. Analyses were performed with PBMCs of patients with MS who had a proliferative response to both MBP and β-synuclein. Numbers of analysed patients are indicated. Data are mean + s.e.m. **f**, Correlation between percentage of $CD4^+$ T cells proliferating in response to the indicated antigens and the grade of disability in patients with MS and Parkinson's disease. Disability was measured by the expanded disability status scale (EDSS) or the Hoehn and Yahr score for patients with MS and Parkinson's disease, respectively. **g**, Correlation between percentage of $CD3^+CD4^+$ T cells proliferating in response to the indicated antigens and the disease duration. **b**, Linear regression analysis. **c**–**e**, Paired two-tailed *t*-test. **f**, **g**, Pearson's r^2. $^*P < 0.05$, $^{**}P < 0.01$, $^{***}P < 0.001$; ns, not significant.

nature research

Corresponding author(s): Alexander Flügel
2018-07-09758C

Reporting Summary

Nature Research wishes to improve the reproducibility of the work that we publish. This form provides structure for consistency and transparency in reporting. For further information on Nature Research policies, see Authors & Referees and the Editorial Policy Checklist.

Statistical parameters

When statistical analyses are reported, confirm that the following items are present in the relevant location (e.g. figure legend, table legend, main text, or Methods section).

n/a	Confirmed	
☐	☒	The exact sample size (*n*) for each experimental group/condition, given as a discrete number and unit of measurement
☐	☒	An indication of whether measurements were taken from distinct samples or whether the same sample was measured repeatedly
☐	☒	The statistical test(s) used AND whether they are one- or two-sided *Only common tests should be described solely by name; describe more complex techniques in the Methods section.*
☐	☒	A description of all covariates tested
☐	☒	A description of any assumptions or corrections, such as tests of normality and adjustment for multiple comparisons
☐	☒	A full description of the statistics including central tendency (e.g. means) or other basic estimates (e.g. regression coefficient) AND variation (e.g. standard deviation) or associated estimates of uncertainty (e.g. confidence intervals)
☐	☒	For null hypothesis testing, the test statistic (e.g. *F*, *t*, *r*) with confidence intervals, effect sizes, degrees of freedom and *P* value noted *Give P values as exact values whenever suitable.*
☒	☐	For Bayesian analysis, information on the choice of priors and Markov chain Monte Carlo settings
☒	☐	For hierarchical and complex designs, identification of the appropriate level for tests and full reporting of outcomes
☐	☒	Estimates of effect sizes (e.g. Cohen's *d*, Pearson's *r*), indicating how they were calculated
☐	☒	Clearly defined error bars *State explicitly what error bars represent (e.g. SD, SE, CI)*

Our web collection on statistics for biologists may be useful.

Software and code

Policy information about availability of computer code

Data collection

Cell Quest Pro (BD)
FACS Diva (BD)
Cytoflex (BC)
AxioVision (r4.8.2, Carl Zeiss MicroImaging)
VS-ASW (Olympus Corp)
Zen 2011 SP3 (Carl Zeiss) v8.1.11.484
MRI (see below)
OneStep real-time PCR (Applied Biosystems) - v2.3
Magellan (Tecan) - v6.6
MicroBeta TriLux (PerkinElmer Life Sciences)
BZ-II Analyzer Software (Keyence)

Data analysis	- FIJI image processing software (NIH) - v2.0.0-rc-59/1.51n - Imaris (Bitplane) - v8.0.1 - FlowJo (FlowJo LLC) - v.10 - Prism (GraphPad Software, Inc) - v7.0a - Excel (MicrosoftOffice 2010, v14.0.7208.5000) - CytExpert (v 2.3 BC)

For manuscripts utilizing custom algorithms or software that are central to the research but not yet described in published literature, software must be made available to editors/reviewers upon request. We strongly encourage code deposition in a community repository (e.g. GitHub). See the Nature Research guidelines for submitting code & software for further information.

Data

Policy information about availability of data

All manuscripts must include a data availability statement. This statement should provide the following information, where applicable:

- Accession codes, unique identifiers, or web links for publicly available datasets
- A list of figures that have associated raw data
- A description of any restrictions on data availability

The data will be available without restriction

Field-specific reporting

Please select the best fit for your research. If you are not sure, read the appropriate sections before making your selection.

☒ Life sciences ☐ Behavioural & social sciences ☐ Ecological, evolutionary & environmental sciences

For a reference copy of the document with all sections, see nature.com/authors/policies/ReportingSummary-flat.pdf

Life sciences study design

All studies must disclose on these points even when the disclosure is negative.

Sample size	Sample sizes were chosen on the basis of standard power calculations (with $\alpha = 0.05$ and power of 0.8) performed for similar experiments that were previously published. In general, statistical methods were not used to re-calculate or predetermine sample sizes.
Data exclusions	No samples were excluded from the analysis.
Replication	Number of reliable reproductions of each experimental finding is stated in each figure legend.
Randomization	Animals from different cages, but within the same experimental group, were selected to assure randomization.
Blinding	Reported in METHODS

Behavioural & social sciences study design

All studies must disclose on these points even when the disclosure is negative.

Study description	*Briefly describe the study type including whether data are quantitative, qualitative, or mixed-methods (e.g. qualitative cross-sectional, quantitative experimental, mixed-methods case study).*
Research sample	*State the research sample (e.g. Harvard university undergraduates, villagers in rural India) and provide relevant demographic information (e.g. age, sex) and indicate whether the sample is representative. Provide a rationale for the study sample chosen. For studies involving existing datasets, please describe the dataset and source.*
Sampling strategy	*Describe the sampling procedure (e.g. random, snowball, stratified, convenience). Describe the statistical methods that were used to predetermine sample size OR if no sample-size calculation was performed, describe how sample sizes were chosen and provide a rationale for why these sample sizes are sufficient. For qualitative data, please indicate whether data saturation was considered, and what criteria were used to decide that no further sampling was needed.*
Data collection	*Provide details about the data collection procedure, including the instruments or devices used to record the data (e.g. pen and paper, computer, eye tracker, video or audio equipment) whether anyone was present besides the participant(s) and the researcher, and whether the researcher was blind to experimental condition and/or the study hypothesis during data collection.*
Timing	*Indicate the start and stop dates of data collection. If there is a gap between collection periods, state the dates for each sample cohort.*

Data exclusions	*If no data were excluded from the analyses, state so OR if data were excluded, provide the exact number of exclusions and the rationale behind them, indicating whether exclusion criteria were pre-established.*
Non-participation	*State how many participants dropped out/declined participation and the reason(s) given OR provide response rate OR state that no participants dropped out/declined participation.*
Randomization	*If participants were not allocated into experimental groups, state so OR describe how participants were allocated to groups, and if allocation was not random, describe how covariates were controlled.*

Ecological, evolutionary & environmental sciences study design

All studies must disclose on these points even when the disclosure is negative.

Study description	*Briefly describe the study. For quantitative data include treatment factors and interactions, design structure (e.g. factorial, nested, hierarchical), nature and number of experimental units and replicates.*
Research sample	*Describe the research sample (e.g. a group of tagged Passer domesticus, all Stenocereus thurberi within Organ Pipe Cactus National Monument), and provide a rationale for the sample choice. When relevant, describe the organism taxa, source, sex, age range and any manipulations. State what population the sample is meant to represent when applicable. For studies involving existing datasets, describe the data and its source.*
Sampling strategy	*Note the sampling procedure. Describe the statistical methods that were used to predetermine sample size OR if no sample-size calculation was performed, describe how sample sizes were chosen and provide a rationale for why these sample sizes are sufficient.*
Data collection	*Describe the data collection procedure, including who recorded the data and how.*
Timing and spatial scale	*Indicate the start and stop dates of data collection, noting the frequency and periodicity of sampling and providing a rationale for these choices. If there is a gap between collection periods, state the dates for each sample cohort. Specify the spatial scale from which the data are taken*
Data exclusions	*If no data were excluded from the analyses, state so OR if data were excluded, describe the exclusions and the rationale behind them, indicating whether exclusion criteria were pre-established.*
Reproducibility	*Describe the measures taken to verify the reproducibility of experimental findings. For each experiment, note whether any attempts to repeat the experiment failed OR state that all attempts to repeat the experiment were successful.*
Randomization	*Describe how samples/organisms/participants were allocated into groups. If allocation was not random, describe how covariates were controlled. If this is not relevant to your study, explain why.*
Blinding	*Describe the extent of blinding used during data acquisition and analysis. If blinding was not possible, describe why OR explain why blinding was not relevant to your study.*

Did the study involve field work? ☐ Yes ☐ No

Field work, collection and transport

Field conditions	*Describe the study conditions for field work, providing relevant parameters (e.g. temperature, rainfall).*
Location	*State the location of the sampling or experiment, providing relevant parameters (e.g. latitude and longitude, elevation, water depth).*
Access and import/export	*Describe the efforts you have made to access habitats and to collect and import/export your samples in a responsible manner and in compliance with local, national and international laws, noting any permits that were obtained (give the name of the issuing authority, the date of issue, and any identifying information).*
Disturbance	*Describe any disturbance caused by the study and how it was minimized.*

Reporting for specific materials, systems and methods

Materials & experimental systems

n/a	Involved in the study
☒	☐ Unique biological materials
☐	☒ Antibodies
☐	☒ Eukaryotic cell lines
☒	☐ Palaeontology
☐	☒ Animals and other organisms
☐	☒ Human research participants

Methods

n/a	Involved in the study
☒	☐ ChIP-seq
☐	☒ Flow cytometry
☐	☒ MRI-based neuroimaging

Unique biological materials

Policy information about availability of materials

Obtaining unique materials: *Describe any restrictions on the availability of unique materials OR confirm that all unique materials used are readily available from the authors or from standard commercial sources (and specify these sources).*

Antibodies

Antibodies used: Reported in METHODS

Validation: *Describe the validation of each primary antibody for the species and application, noting any validation statements on the manufacturer's website, relevant citations, antibody profiles in online databases, or data provided in the manuscript.*

Eukaryotic cell lines

Policy information about cell lines

Cell line source(s): GP+E86 ecotropic retroviral packaging cell line (ATCC).
Lewis rat CD4 effector T cell lines specific for myelin basic protein (this study).
Lewis rat CD4 effector T cell lines specific for beta-synuclein (this study).
Lewis rat CD4 effector T cell lines specific for ovalbumin (this study).

Authentication: No authentication was performed for GP+E86 and derivative cell lines.
For T cell lines, authentication reported in METHODS. For T cell lines characterization see Ext Data Fig. 1

Mycoplasma contamination: All used cell lines were tested negative for mycoplasma contamination.

Commonly misidentified lines (See ICLAC register): *Name any commonly misidentified cell lines used in the study and provide a rationale for their use.*

Palaeontology

Specimen provenance: *Provide provenance information for specimens and describe permits that were obtained for the work (including the name of the issuing authority, the date of issue, and any identifying information).*

Specimen deposition: *Indicate where the specimens have been deposited to permit free access by other researchers.*

Dating methods: *If new dates are provided, describe how they were obtained (e.g. collection, storage, sample pretreatment and measurement), where they were obtained (i.e. lab name), the calibration program and the protocol for quality assurance OR state that no new dates are provided.*

☐ Tick this box to confirm that the raw and calibrated dates are available in the paper or in Supplementary Information.

Animals and other organisms

Policy information about studies involving animals; ARRIVE guidelines recommended for reporting animal research

Laboratory animals: Lewis rats on a LEW/Crl background were bred at the animal facility of the University Medical Centre Göttingen (Germany) or obtained from Charles River (Germany). T cell receptor transgenic Lewis rat strain (ubiquitous expression of GFP-TCRa-TCRb transgene; unknown integration site) specific for beta-synuclein antigen was generated in this study and maintained at the animal facility of University Medical Centre Göttingen.

Wild animals: *Provide details on animals observed in or captured in the field; report species, sex and age where possible. Describe how animals were caught and transported and what happened to captive animals after the study (if killed, explain why and describe method; if released, say where and when) OR state that the study did not involve wild animals.*

Field-collected samples	*For laboratory work with field-collected samples, describe all relevant parameters such as housing, maintenance, temperature, photoperiod and end-of-experiment protocol OR state that the study did not involve samples collected from the field.*

Human research participants

Policy information about studies involving human research participants

Population characteristics	Described in the text (Ext. Data. Fig.10)
Recruitment	The patients were recruited by a clinician in a random way

ChIP-seq

Data deposition

☐ Confirm that both raw and final processed data have been deposited in a public database such as GEO.

☐ Confirm that you have deposited or provided access to graph files (e.g. BED files) for the called peaks.

Data access links *May remain private before publication.*	*For "Initial submission" or "Revised version" documents, provide reviewer access links. For your "Final submission" document, provide a link to the deposited data.*
Files in database submission	*Provide a list of all files available in the database submission.*
Genome browser session (e.g. UCSC)	*Provide a link to an anonymized genome browser session for "Initial submission" and "Revised version" documents only, to enable peer review. Write "no longer applicable" for "Final submission" documents.*

Methodology

Replicates	*Describe the experimental replicates, specifying number, type and replicate agreement.*
Sequencing depth	*Describe the sequencing depth for each experiment, providing the total number of reads, uniquely mapped reads, length of reads and whether they were paired- or single-end.*
Antibodies	*Describe the antibodies used for the ChIP-seq experiments; as applicable, provide supplier name, catalog number, clone name, and lot number.*
Peak calling parameters	*Specify the command line program and parameters used for read mapping and peak calling, including the ChIP, control and index files used.*
Data quality	*Describe the methods used to ensure data quality in full detail, including how many peaks are at FDR 5% and above 5-fold enrichment.*
Software	*Describe the software used to collect and analyze the ChIP-seq data. For custom code that has been deposited into a community repository, provide accession details.*

Flow Cytometry

Plots

Confirm that:

☐ The axis labels state the marker and fluorochrome used (e.g. CD4-FITC).

☒ The axis scales are clearly visible. Include numbers along axes only for bottom left plot of group (a 'group' is an analysis of identical markers).

☐ All plots are contour plots with outliers or pseudocolor plots.

☐ A numerical value for number of cells or percentage (with statistics) is provided.

Methodology

Sample preparation	Reported in Methods
Instrument	BD FACSCalibur, BD FACS Aria II, Cytoflex
Software	CellQuest Pro, CytExpert or BD FACS Diva software were used for acquisition of flow cytometry data
Cell population abundance	*Describe the abundance of the relevant cell populations within post-sort fractions, providing details on the purity of the samples and how it was determined.*

Gating strategy | *Describe the gating strategy used for all relevant experiments, specifying the preliminary FSC/SSC gates of the starting cell population, indicating where boundaries between "positive" and "negative" staining cell populations are defined.*

☐ Tick this box to confirm that a figure exemplifying the gating strategy is provided in the Supplementary Information.

Magnetic resonance imaging

Experimental design

Design type	'Described in the respective Figure legends and the Method section
Design specifications	not applicable
Behavioral performance measures	not applicable

Acquisition

Imaging type(s)	structural
Field strength	9.4 T
Sequence & imaging parameters	T2-weighted axial MRI with repetition time (TR) of 9286 ms, echo time (TE) of 11 ms, RARE factor of 12, 60 slices, in-plane resolution of 120×120 µm, slice thickness of 480 µm, and total acquisition time (TA) of 195 s as well as sagittal MRI (TR/TE = 4333/11 ms, RARE factor = 12, 28 slices, field-of-view = 30.72×30.72 mm, matrix size = 256×256, in-plane resolution = 120×60 µm, slice thickness = 480 µm, and TA = 182 s) were performed with the use of multislice fast spin-echo MRI. T1-weighted fat-suppressed sagittal gradient-echo MRI (3D FLASH, TR/TE = 14.8/4.2 ms, flip angle = 25°, and TA = 16 min) was performed at an isotropic resolution of 120 µm (field-of-view = 30.72×30.72×30.72mm, matrix size = 256×256) before and after an intravenous injection of Gadobutrol solution.
Area of acquisition	Brain

Diffusion MRI ☐ Used ☒ Not used

Preprocessing

Preprocessing software	not applicable
Normalization	not applicable
Normalization template	not applicable
Noise and artifact removal	not applicable
Volume censoring	not applicable

Statistical modeling & inference

Model type and settings	not applicable
Effect(s) tested	not applicable

Specify type of analysis: ☐ Whole brain ☒ ROI-based ☐ Both

Statistic type for inference (See Eklund et al. 2016)	not applicable
Correction	not applicable

Models & analysis

n/a	Involved in the study
☒	☐ Functional and/or effective connectivity
☒	☐ Graph analysis
☒	☐ Multivariate modeling or predictive analysis

Functional and/or effective connectivity	*Report the measures of dependence used and the model details (e.g. Pearson correlation, partial correlation, mutual information).*
Graph analysis	*Report the dependent variable and connectivity measure, specifying weighted graph or binarized graph, subject- or group-level, and the global and/or node summaries used (e.g. clustering coefficient, efficiency, etc.).*

Multivariate modeling and predictive analysis

Specify independent variables, features extraction and dimension reduction, model, training and evaluation metrics.